

# Zeta potential of CO<sub>2</sub>-rich aqueous solutions in contact with intact sandstone sample at temperatures of 23°C and 40°C and pressures up to 10.0 MPa

Miftah Hidayat<sup>a,b</sup>, Mohammad Sarmadivaleh<sup>b</sup>, Jos Derksen<sup>a</sup>, David Vega-Maza<sup>a,c</sup>, Stefan Iglauer<sup>d,e</sup> and Jan Vinogradov<sup>a</sup>

<sup>a</sup> University of Aberdeen, School of Engineering, Elphinstone Road, AB24 3UE Aberdeen, United Kingdom

<sup>b</sup> Curtin University, Discipline of Petroleum Engineering, 26 Dick Perry Avenue, 6151 Kensington, Australia

<sup>c</sup> Now at University of Valladolid, School of Engineering. TermoCal, BioEcoUva Institute. Valladolid, Spain

<sup>d</sup> Edith Cowan University, Centre for Sustainable Energy and Resources, 270 Joondalup Drive, 6027 Joondalup, Australia

<sup>e</sup> Edith Cowan University, School of Engineering, 270 Joondalup Drive, 6027 Joondalup, Australia

## Abstract

Despite the broad range of interest and applications, controls on the electric surface charge and the zeta potential of silica in contact with aqueous solutions saturated with dissolved CO<sub>2</sub> at conditions relevant to natural systems, remains unreported. There have been no published zeta potential measurements conducted in such systems at equilibrium, hence the effect of composition, pH, temperature and pressure remains unknown.

We describe a novel methodology developed for the streaming potential measurements under these conditions, and report zeta potential values for the first time obtained with Fontainebleau sandstone core sample saturated with carbonated NaCl, Na<sub>2</sub>SO<sub>4</sub>, CaCl<sub>2</sub> and MgCl<sub>2</sub> solutions under equilibrium conditions at pressures up to 10 MPa and temperatures up to 40°C.

The results demonstrate that pH of solutions is the only control on the zeta potential, while temperature, CO<sub>2</sub> pressure and salt type affect pH values. We report three empirical relationships that describe the pH dependence of the zeta potential for: i) dead (partial CO<sub>2</sub> pressure of 10<sup>-3.44</sup> atm) NaCl/Na<sub>2</sub>SO<sub>4</sub>, ii) dead CaCl<sub>2</sub>/MgCl<sub>2</sub> solutions, and iii) for all live (fully saturated with dissolved CO<sub>2</sub>) solutions. The proposed new relationships provide essential insights into interfacial electrochemical properties of silica-water systems at conditions relevant to CO<sub>2</sub> geological storage.

## 1. Introduction

Quartz is a common mineral comprising 12% of the Earth's crust [1]. Quartz is also the constituent mineral of sandstone formations, and it can be found in many subsurface settings including aquifers (e.g., [2,3]), hydrocarbon reservoirs (e.g., [4,5]) and geothermal sources (e.g., [6,7]). To characterize the subsurface flows in such settings, a variety of electrical geophysical methods are available including electrical resistivity tomography (e.g., [8,9]), electro-seismic (injecting electric current and measuring the resulting seismic energy; e.g., [10,11]), seismo-electric (generating a seismic wave and measuring the resulting electric field; e.g., [11,12]) and self-potential (SP) (voltage that arises in response to existing gradients in pressure, concentration or temperature; e.g., [13,14]) measurement. The SP has been shown to be an efficient method to characterize single- and multi-phase flows in the subsurface, especially in sandstone reservoirs (e.g., [15,16]). Moreover, the SP method can characterize permeability heterogeneities (e.g., fractures, faults, and variable permeability zones [17,18]).

46 The SP method relies on electrochemical processes that arise in response to the  
47 establishment of an electrical double layer (EDL) at the rock-water interface; this can be  
48 characterized by the zeta potential (e.g., [19,20]). The zeta potential also plays an important  
49 role in determining the wettability (e.g., [21]); while the wetting state controls the pore  
50 occupancy of aqueous solutions (hereafter referred to as water for simplicity) and non-  
51 aqueous phase fluids (NAPF) in multi-phase systems, and thus strongly influences fluid  
52 saturations and flow patterns, e.g. in CO<sub>2</sub> geological storage (CGS) [22], hydrocarbon  
53 recovery [23], or H<sub>2</sub> geo-storage [24].

54 There are three principal forces (namely van der Waals, structural and electrostatic forces  
55 [25]) that act between rock-water and NAPF-water interfaces; these forces determine the  
56 disjoining pressure, which in turn controls the wetting state. Structural forces are always  
57 repulsive, thus implying a positive (repulsive) contribution to the disjoining pressure [25,26],  
58 while van der Waals forces depend on properties of all constituent phases (refractive index,  
59 dielectric constant and absorption frequency), and these forces can be characterized by the  
60 Hamaker theory, resulting in either positive or negative [25,27,28] to the disjoining pressure.  
61 Electrostatic forces can also be positive or negative [25,29] depending on rock mineralogy,  
62 water pH, ionic strength and chemical composition. The magnitude and polarity of the  
63 electrostatic forces depend on the interfacial zeta potentials, which can vary substantially [26],  
64 therefore these forces play a key role in controlling the wettability.

65 In order to accurately characterize the wettability, the measured experimental data of zeta  
66 potential of rock-water and NAPF-water interfaces is essential. There are two common  
67 methods available for measuring zeta potential; namely the electrophoretic mobility and  
68 streaming potential. The electrophoretic mobility method (EPM) relies on the motion of the  
69 dispersed phase (either rock or NAPF) relative to the continuous stationary water phase under  
70 the influence of an applied electric field [30]. In contrast, the streaming potential method (SPM)  
71 is based on the flow of water through a stationary porous medium, which may also contain  
72 NAPF, under the influence of a pressure gradient [20,30]. The benefits of using EPM include  
73 a relative ease of use commercially available instruments. However, the measurement  
74 conditions are far from representative of deep subsurface settings for several reasons. Firstly,  
75 EPM cannot currently be used under high pressure and elevated temperature conditions, or  
76 with high ionic strength electrolytes (>1M; M = mol·L<sup>-1</sup>), the conditions that are typical for deep  
77 rock formations [26]. Secondly, EPM requires either a powdered mineral sample or emulsified  
78 NAPF dispersed in water and therefore, it cannot capture the true complex pore space  
79 topology [26]. Finally, EPM cannot take into account a third phase, which is needed for multi-  
80 phase flow (e.g., water and gas) [31]. In contrast, SPM can be used on intact sandstone  
81 samples (e.g., [32,33]), at elevated temperature (e.g., [16]), using low-to-high salinity  
82 electrolytes of simple and complex composition (e.g., [34]) and also on multi-phase systems  
83 containing water, NAPF and minerals at the same time (e.g., [35,36]). However, conducting  
84 SPM experiments is challenging and time consuming. In addition, to the best of our  
85 knowledge, thus far there has been no published study that reported either EPM or SPM zeta  
86 potential measurements under high pore pressure and elevated temperature conditions,  
87 typical for deep subsurface settings. Acquisition of the high pore pressure and elevated  
88 temperature data is particularly important as gas under these conditions (e.g., CO<sub>2</sub> during  
89 carbon dioxide sequestration or CO<sub>2</sub> injection for improved oil recovery) dissolves in water to  
90 a higher degree and alters the ionic composition, reduces pH, so that the resulting aqueous  
91 solution becomes the so-called carbonated water (C<sub>water</sub>). Such changes in water chemistry  
92 will have an impact on the C<sub>water</sub>-rock and C<sub>water</sub>-NAPF zeta potentials and will ultimately  
93 affect the wettability and dynamics of flow of each fluid. Note, that the term C<sub>water</sub> used in  
94 this study corresponds to any aqueous solution with non-zero concentration of dissolved CO<sub>2</sub>.

95 Several attempts have been made to measure the zeta potential in CO<sub>2</sub> containing systems.  
1 96 A recent study published by Kim and Kwak [37] reported the zeta potential of CO<sub>2</sub>-water  
2 97 interfaces using EPM. The experiments were conducted by bubbling CO<sub>2</sub> gas through 0.01M  
3 98 NaCl solution. The zeta potential was reported to be negative, but the experiments were  
4 99 conducted at atmospheric pressure and unreported temperature. Another study by Moore et  
5 100 al. [38] reported measurements of the zeta potential using SPM in Berea sandstone samples  
6 101 saturated with tap water and liquid CO<sub>2</sub>. The experiments were conducted at a maximum  
7 102 pressure of 6.5 MPa and temperature of 20°C, so that the latter value is not consistent with  
8 103 the expected temperature of 38°C normally found at the depth that corresponds to 6.5 MPa  
9 104 [39]. The single-phase zeta potential was measured in rock sample fully saturated with water,  
10 105 which was not carbonated prior to the experiments, i.e., the amount of dissolved CO<sub>2</sub>  
11 106 corresponded to the atmospheric level. The experiment was repeated with water and  
12 107 immiscible liquid CO<sub>2</sub> and the effective (i.e., multi-phase) zeta potential was found to be  
13 108 negative and approximately ten-fold smaller in magnitude compared with the single-phase  
14 109 zeta potential. However, Moore et al. [38] did not report single-phase zeta potential  
15 110 measurements conducted with C<sub>water</sub> under the same experimental conditions, hence the  
16 111 contribution of the zeta potential at the interface between water and immiscible liquid CO<sub>2</sub>  
17 112 could not be quantified. Moreover, Moore et al. [38] did not report the equilibrium pH of water  
18 113 during the experiments, to indicate whether chemical equilibrium between the mineral, water  
19 114 and liquid CO<sub>2</sub> was established. Since pH is known to have a strong effect on the silica-water  
20 115 zeta potential [16,40], uncertainty exists in relation to Moore et al.'s [38] reported multi-phase  
21 116 zeta potential results. Furthermore, to the best of our knowledge, no experimental zeta  
22 117 potential data for C<sub>water</sub>-rock or C<sub>water</sub>-immiscible CO<sub>2</sub> interfaces under high pressure  
23 118 and elevated temperature conditions has been reported (which are typical for deep subsurface  
24 119 formations). Note that in CGS, CO<sub>2</sub> is stored below a depth of 800 m, so that the CO<sub>2</sub> exists  
25 120 in a dense supercritical phase [41,42] which correspond to the critical point of CO<sub>2</sub> is 7.38 MPa  
26 121 and 31.1°C).

33 122 In the absence of such measured zeta potential data, several models have been proposed  
34 123 with which the wettability of sandstones can be predicted. For instance, Tokunaga [43] and  
35 124 Kim et al. [44] reported an analytical model of water film stability, based on DLVO (Derjaguin,  
36 125 Landau, Verwey, Overbeek) theory; the model was used to simulate CO<sub>2</sub> geological storage  
37 126 (CGS) conditions in sandstone reservoirs. The model required knowledge of the electrostatic  
38 127 interactions between silica-water and CO<sub>2</sub>-water interfaces, to calculate the corresponding  
39 128 contribution to the disjoining pressure, and the model was implemented using compression  
40 129 approximation [45]. Tokunaga [43] and Kim et al. [44] assumed that the zeta potential of the  
41 130 silica-water interface was -25 mV for 0.01 M ionic strength solution, and -5 mV for 2 M ionic  
42 131 strength. Both, Tokunaga [43] and Kim et al. [44] assumed a zero zeta potential at the CO<sub>2</sub>-  
43 132 water interface. However, neither of the assumed values was validated due to a lack of  
44 133 experimental data under true CGS conditions. Moreover, when the CO<sub>2</sub> dissolves in water at  
45 134 high pressure, and the pH of C<sub>water</sub> becomes substantially lower [46,47], the zeta potential  
46 135 of C<sub>water</sub>-silica interfaces should become vanishingly small [48]. This, however, is  
47 136 inconsistent with the assumed values by Tokunaga [43] and Kim et al. [44], thus their  
48 137 wettability estimates are also doubtful.

53 138 Therefore, the main aim of this study is to develop an experimental methodology and for the  
54 139 first time measure the streaming potentials in intact sandstone samples under high pressure  
55 140 and elevated temperature, using C<sub>water</sub>, to improve our understanding of the  
56 141 electrochemical processes that take place at silica-water interfaces. The outcomes of this  
57 142 study will, among other applications, better inform CGS, hydrocarbon recovery and

geothermal projects. This work also provides fundamental petrophysical data essential for a broad range of Earth sciences.

## 2. Materials and methods

### 2.1. Materials

A cylindrical Fontainebleau sandstone sample was used in this study. Petrophysical properties of the sample listed in **Table 1** suggest partial cementation, in line with the values of porosity and formation factor [32], which was important for repeated saturation. Prior to conducting the streaming potential measurements, the sample was thoroughly cleaned following the procedure reported by Alroudhan et al. [31].

Sample	Fontainebleau sandstone
Mineralogy	>99 wt% quartz
Porosity	9.0 ± 1.0%
Liquid Permeability	70 ± 5 mD ( $6.91 \times 10^{-14} \pm 4.93 \times 10^{-15} \text{ m}^2$ )
Dimensions	Length = 0.0783 m, Diameter = 0.0382 m
Formation Factor, <i>F</i>	58±2

**Table 1.** Petrophysical properties of the Fontainebleau sandstone sample used in this study. Mineralogy of the sample was taken from [34,49,50]. Sample porosity was measured by gas (N<sub>2</sub>) expansion using AP-608 Automated Permeameter and Porosimeter (Coretest System Inc, USA). The formation factor was obtained with five dead NaCl solutions with ionic strength between 0.05 M and 1 M. The liquid permeability was calculated using Darcy's Law from the slope of linear regression of the flow rate against the pressure difference during the streaming potential measurements using at least four different flow rates with confirmed high quality of regression ( $R^2 \geq 0.98$ ).

We used synthetic single-salt solutions made with reagent-grade NaCl, CaCl<sub>2</sub>·2H<sub>2</sub>O, MgCl<sub>2</sub>·6H<sub>2</sub>O, and Na<sub>2</sub>SO<sub>4</sub> (Sigma Aldrich, Australia) dissolved in deionized (DI) water. The DI water (electrical resistivity 15 MΩ·cm -18 MΩ·cm) was supplied by a filtering system from Ibis Technology (Ascot, Australia). The ionic strength of all four solutions was kept constant at 0.05 M during preparation under laboratory (ambient) pressure and 23°C temperature. All laboratory experiments were conducted using two types of aqueous solutions: 'dead' and 'live' water. The dead water was a synthetic aqueous solution fully equilibrated with atmospheric CO<sub>2</sub> (which corresponds to partial CO<sub>2</sub> pressure of 10<sup>-3.44</sup> atm and to a dissolved CO<sub>2</sub> concentration of 1.487 × 10<sup>-5</sup> M [51]). The CO<sub>2</sub> content of the dead water remained unchanged throughout the experiment. On the other hand, to prepare the live water we used a salt solution prepared under ambient pressure and temperature, which subsequently was brought in contact with pure CO<sub>2</sub> (supplied by Coregas, Australia, with the mole fraction ≥ 0.99) in a mixing reactor [52]. The system was pressured and heated to target experimental pressure and temperature. Allowing CO<sub>2</sub> and water to mix for a long period of time in the reactor (no less than 3 hours); while measuring the volume of the CO<sub>2</sub> cap until it stabilized under constant pressure, the thermodynamic equilibrium between water and CO<sub>2</sub> was established. The target pressure and temperature that corresponded to the live water equilibrium was maintained throughout each experiment.

Prior to carrying out the streaming potential measurements with dead water, the saturated rock sample was placed in a core holder, and the entire system was sealed from atmosphere. The detailed experimental protocol of the streaming potential measurement using both dead and live water is provided in subsequent sections.

### 2.2. Measurements of pH and, water and saturated rock electrical conductivity

The dead water experiments were conducted at pore pressures up to 10 MPa and temperatures up to 40°C. Since the concentration of dissolved CO<sub>2</sub> remained constant at atmospheric level during the dead water experiments (in the closed system), effluent water samples were regularly collected and pH values and electrical conductivities were measured

186 outside the system using a FiveGo pH meter (Mettler Toledo, accuracy of 0.01 pH units) and  
 187 a Jenway 4520 conductivity meter (Cole-Palmer, 0.5% accuracy), respectively.

188 The live water experiments were carried out over the same pressure ranges (up to 10 MPa  
 189 backpressure) and temperatures of 40°C. Live water pH values were measured using an in-  
 190 line high-pressure pH meter (Corr Instruments, LLC). Both pH meters, as well as the  
 191 conductivity meter were regularly calibrated using standard solutions and manufacturer's  
 192 recommended procedure.

193 The chemical equilibrium between the rock sample and all aqueous solutions was assured  
 194 using pH and water electrical conductivity measurements on a regular basis as detailed by  
 195 Vinogradov and Jackson [16]. Therefore, the measured pH values and water conductivities  
 196 reported here represent the equilibrium values (for a given solution, pressure and  
 197 temperature). Dead and live water properties are provided in **Table 2**.

198 The saturated rock conductivity ( $\sigma_{rw}$ ) was measured in-situ using a pair of internal electrodes  
 199 and following the procedure of Vinogradov et al. [34]. The intrinsic formation factor ( $F$ ) was  
 200 obtained prior to carrying out the streaming potential measurements using NaCl solutions  
 201 between 0.05M and 1M, and following the protocol of Vinogradov et al. [34].

### 202 2.3. Experimental setup

203 The streaming potential measurements were conducted in a high pressure-high temperature  
 204 (HPHT) coreflooding apparatus (schematically shown in **Figure 1**). The coreflooding  
 205 apparatus was placed inside an oven with controlled temperature (accuracy of  $\pm 1^\circ\text{C}$ ). For the  
 206 dead water experiments, the branch of the experimental apparatus comprising units #10 - #12  
 207 (**Fig.1**), used for preparing live water, was disconnected from the rest of the setup.

208 The pressure difference across the core sample was measured continuously with a high  
 209 precision Keller-Druck pressure transducers (0.1% accuracy). Furthermore, the voltage  
 210 across the sample was recorded with a NI 9207 voltmeter with high internal impedance ( $>1$   
 211 G $\Omega$ ) and 0.52% accuracy. Two high precision syringe pumps (#1 in **Fig.1**; 500D Hastelloy  
 212 ISCO) were used as injector and receiver to induce water flow in either direction through the  
 213 sample. The pump used as injector was set to deliver water at a constant flow rate while the  
 214 receiving pump on the opposite side was set at a constant receiving pressure (i.e., maintaining  
 215 a constant back pressure during the experiment). During all coreflooding experiments, the  
 216 difference between the confining pressure and the pore pressure was kept constant at  
 217 approximately 3 MPa. The maximum difference between the injection and the outlet pressure  
 218 that corresponds to the highest tested flow rate was 0.14 MPa. Constant target temperature  
 219 was maintained during the experiments by heating cylinders of both pumps with an embedded  
 220 water jacket and insulating all flowlines outside the oven to prevent heat losses. Upon  
 221 completion of each streaming potential experiment, the saturated rock conductivity was  
 222 measured using the internal electrodes (#8) connected to a BK Precision 891 LCR meter  
 223 (0.05% accuracy), by sweeping the applied alternate voltage frequency between 20 Hz and  
 224 300 KHz.

Solution	P, MPa	T, °C	Solution type	pH value	$\sigma_w$ , S/m
NaCl	0.2	23	Dead water	7.10 $\pm$ 0.10	0.55
	4.5	23	Dead water	7.00 $\pm$ 0.10	0.55
	7.5	23	Dead water	7.10 $\pm$ 0.10	0.56
	10.0	23	Dead water	7.20 $\pm$ 0.10	0.55
	0.2	40	Dead water	6.30 $\pm$ 0.20	0.61
	4.5	40	Dead water	6.30 $\pm$ 0.20	0.60

	7.5	40	Dead water	6.20 ± 0.20	0.61
	10	40	Dead water	6.20 ± 0.20	0.60
	4.5	40	Live water	3.80 ± 0.10	0.65
	7.5	40	Live water	3.50 ± 0.10	0.64
	10.0	40	Live water	3.33 ± 0.05	0.55
CaCl <sub>2</sub>	0.2	23	Dead water	6.20 ± 0.10	0.34
	7.5	23	Dead water	6.20 ± 0.10	0.34
	0.2	40	Dead water	5.60 ± 0.20	0.46
	7.5	40	Dead water	5.50 ± 0.20	0.46
	7.5	40	Live water	3.17 ± 0.05	0.54
MgCl <sub>2</sub>	0.2	23	Dead water	6.90 ± 0.10	0.37
	7.5	23	Dead water	6.80 ± 0.10	0.37
	0.2	40	Dead water	6.05 ± 0.20	0.51
	7.5	40	Dead water	6.10 ± 0.20	0.51
	7.5	40	Live water	3.40 ± 0.05	0.50
Na <sub>2</sub> SO <sub>4</sub>	0.2	23	Dead water	7.80 ± 0.10	0.36
	7.5	23	Dead water	7.70 ± 0.10	0.36
	0.2	40	Dead water	6.70 ± 0.20	0.48
	7.5	40	Dead water	6.70 ± 0.20	0.48
	7.5	40	Live water	3.60 ± 0.10	0.59

**Table 2.** Dead and live water properties for all tested experimental conditions, where  $P$  is the pore pressure,  $T$  is the experimental temperature,  $\sigma_w$  is the electrical conductivity of tested solution. pH values reported for all dead water experiments correspond to partial  $\text{CO}_2$  pressure of  $10^{-3.44}$  atm. The ionic strength of all solution was kept constant at 0.05 M. The reported uncertainties in the table are based on both the instrument accuracy and measurement repeatability. The total uncertainty in  $\sigma_w$  was  $\pm 0.01$  S/m in all experiments.

#### 2.4. Streaming potential measurements in rock samples saturated with dead water

The streaming potential method was used to obtain the zeta potential of the rock-water interface. The method relies on the assumption that at steady state, the streaming current is balanced by the conduction current during one-directional flow of water through the porous medium, consistent with our core flooding experiments where stable pressure and voltage were established across the rock sample. To achieve such conditions, the paired-stabilized (PS) method described in Vinogradov and Jackson [36] was implemented to measure the streaming potential coupling coefficient ( $C_{SP}$ ). Employing the PS method also allowed us to eliminate any asymmetry in the electrode potential as detailed in [34].  $C_{SP}$  was interpreted from the slope of linear regression of stabilized (normalized) voltage (see Equation 7a in Vinogradov et al. [34]) as a function of stabilized pressure difference (normalized  $\Delta P$ ; see Equation 7b in Vinogradov et al. [34]). The zeta potential ( $\zeta$ ) was then calculated via the modified Helmholtz-Smoluchowski equation (which accounts for the surface electrical conductivity [20,53,54]):

$$C_{SP} = \frac{\Delta V}{\Delta P} = \frac{\varepsilon \zeta}{\mu \sigma_{rw} F} \quad (1)$$

where  $\Delta V$  is the stabilised voltage in [V],  $\Delta P$  is stabilised pressure [Pa],  $\varepsilon$  is the water permittivity in [ $\text{F}\cdot\text{m}^{-1}$ ],  $\mu$  is the water dynamic viscosity in [ $\text{Pa}\cdot\text{s}$ ],  $\sigma_{rw}$  is the electrical conductivity of the saturated rock sample in [ $\text{S}\cdot\text{m}^{-1}$ ] and  $F$  is the intrinsic formation factor, which was found

248 to be constant for all tested solutions implying negligibly small surface conductivity even at the  
 249 lowest tested ionic strengths (refer to S1 is supplementary material). Note, that since  $F =$   
 250  $\frac{\sigma_w}{\sigma_{rw}} = 58$  was constant for all tested solutions, **Eq. 1** reduces to the classical Helmholtz-  
 251 Smoluchowski equation and water conductivity can also be used to compute the zeta potential.  
 252 We calculated  $\varepsilon$  and  $\mu$  to account for the temperature and ionic strength using the correlations  
 253 provided in Saunders et al. [55].

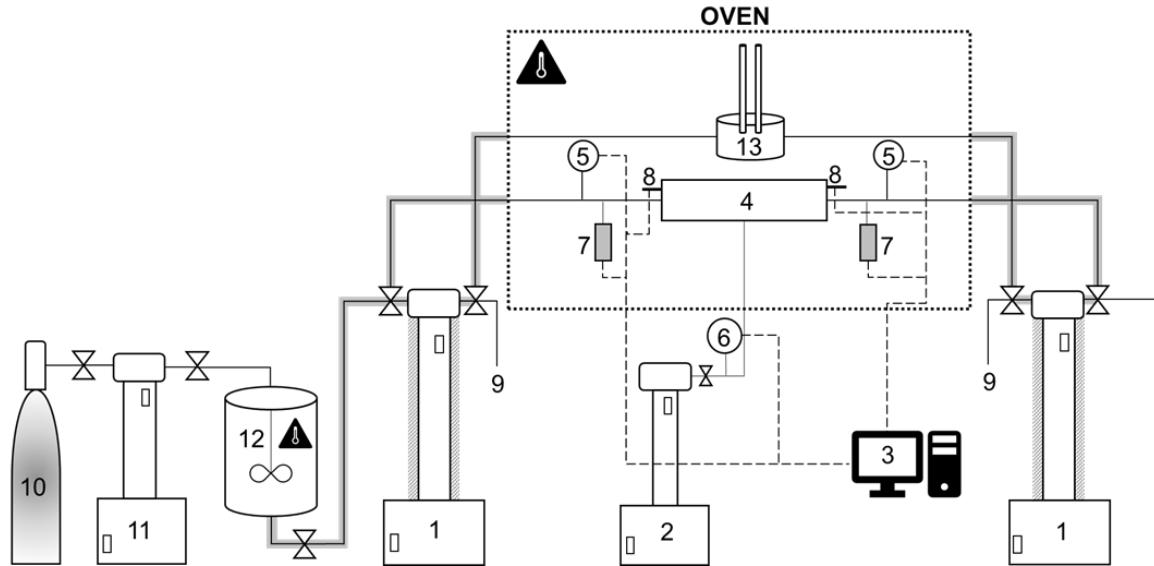


**Figure 1.** The experimental apparatus used in streaming potential measurements. The solid grey lines represent flowlines and the dashed grey lines represent electrical connections. (#1) heated 500D Hastelloy ISCO pumps to the left and to the right of the core holder; (#2) 500D is a stainless steel ISCO pump used to induce the confining pressure around the rock sample; (#3) data acquisition system; (#4) is the HPHT coreflooding cell (core holder); (#5) two high precision pressure transducers; (#6) high precision pressure transducer used to monitor the confining pressure; (#7) external electrodes to the left and to the right of the core holder; (#8) internal electrodes to the left and to the right of the core holder; (#9) are sampling tubes to the left and to the right of the core holder; (#10) CO<sub>2</sub> cylinder; (#11) 260D Stainless steel ISCO pump used for pumping CO<sub>2</sub> into the mixing reactor; (#12) heated Parr mixing reactor; (#13) high pressure in-line pH meter.

## 2.5. Streaming potential measurements in rock samples saturated with live water

The live water experiments required several modifications to the apparatus and the experimental protocol due to the corrosive nature of the live water. The new procedure is detailed below.

During the rock sample preparation step, an additional layer of thin polytetrafluoroethylene (PTFE) tape was wrapped around the rock sample, and a PTFE heat shrinkable sleeve was placed around the PTFE taped sample. The entire assembly was then placed inside a Viton sleeve, which was thus isolated from the corrosive pore fluid. The sample inside the Viton sleeve was mounted into the core holder (#4) and pressurized with dead water as a confining fluid (note, that Viton is not compatible with acids).

For preparing live water, 500 mL dead water were placed in the mixing reactor (#12), and the reactor was closed with a small air cap left at the top of the dead water. The reactor was heated overnight by circulating hot water in its water jacket to the target 40°C at atmospheric pressure so that the experimental temperature was established.

279 Fluid equilibration started with the delivery of CO<sub>2</sub> at 4 MPa from the CO<sub>2</sub> cylinder (#10) to the  
 1 280 pre-empted high precision syringe pump (#11). Subsequently, the CO<sub>2</sub> in the pump was  
 2 281 pressurized to the target pore pressure (4,5 MPa, 7.5 MPa or 10 MPa), and pumped through  
 3 282 flowlines into the mixing reactor using constant pressure delivery mode. The volume of the  
 4 283 CO<sub>2</sub> remaining in the pump (#11) was constantly monitored, and the pressure in the reactor  
 5 284 (#12) was equilibrated with that of the pump (#11) using the constant pressure delivery mode,  
 6 285 and the gas entrainment stirrer inside the reactor was activated to rigorously mix the liquid  
 7 286 phase (water) and the CO<sub>2</sub> cap at the top (thus accelerating the equilibration [52]). Equilibrium  
 8 287 between the water and CO<sub>2</sub> phases was assumed to have been established when the volume  
 9 288 of CO<sub>2</sub> inside the pump ceased to decrease and remained constant for at least 3 hours thus  
 10 289 indicating that no additional CO<sub>2</sub> dissolved in water. At this stage, we assumed the water was  
 11 290 fully saturated with CO<sub>2</sub> and it was transferred from the reactor to the injection pump (#1, to  
 12 291 the left of the core holder in **Fig.1**) for the experiments.

16 292 Due to technical limitations of the injection pump (#1), all of the live water in the reactor (#12)  
 17 293 was transferred to the pump (#1 to left of the core holder in **Fig.1**) containing approximately 5  
 18 294 mL of dead water. Moreover, the setup's dead volumes (valves, tubing), the pore space of the  
 19 295 rock sample, and the receiving pump (#1 to the right of the core holder in **Fig.1**) also contained  
 20 296 pressured (to the same pressure as that in the injection pump) dead water. In total, 400 mL of  
 21 297 fully CO<sub>2</sub> saturated live water was mixed with approximately 30 mL of dead water remaining  
 22 298 in the system, thus disturbing the chemical and thermodynamic equilibrium. Therefore, to re-  
 23 299 equilibrate the system, flow of the mixed solution was induced from left to right and back again.  
 24 300 The procedure that usually lasted for at least 2 days was repeated several times while  
 25 301 regularly measuring the pH, rock permeability, electrical conductivity of the sample and  $C_{SP}$ ,  
 26 302 until all properties stabilized at constant values (within 2% tolerance). The confirmed stability  
 27 303 of electrical conductivity of the saturated rock sample and its permeability throughout the  
 28 304 equilibration period also indicated there was no measurable dissolution or precipitation of  
 29 305 minerals.

33 306 The streaming potential measurements then commenced and were completed using at least  
 34 307 4 different flow rates following the recommended PS procedure [36]. To measure the voltage  
 35 308 across the rock sample in live water experiments only the internal electrodes (#8) were used  
 36 309 (details on design and materials used for the internal electrodes are provided in [34]) due to  
 37 310 their higher stability relative to that of the external electrodes. The zeta potential was  
 38 311 interpreted from the measured  $C_{SP}$  using **Eq.1**, for which the updated values of  $\sigma_{rw}$ ,  $\epsilon$  and  $\mu$  of  
 39 312 live water were required ( $F$  remained constant in all reported single-phase experiments).

42 313 The live water saturated rock conductivity ( $\sigma_{rw}$ ) was measured in each experiment. Live water  
 43 314 electrical conductivity ( $\sigma_w$ ) was calculated by multiplying the intrinsic formation factor  
 44 315 (assumed to be constant and equal to that measured with the corresponding dead water) by  
 45 316 the live water saturated rock conductivity and all values are reported in **Table 2**. The live water  
 46 317 ionic strength (salinity) was determined using  $\sigma_w$  (refer to section 2.6 in Vinogradov et al. [34]),  
 47 318 and the salinity was then used to adjust the permittivity of live water ( $\epsilon$ ) using the approach  
 48 319 described in Saunders et al. [55].

51 320 The viscosity of the live water ( $\mu_{lw}$ ) at given pressure and temperature was then calculated  
 52 321 via the approach proposed by Islam and Carlson [56]:

$$\mu_{lw} = \mu_s \times (1 + 4.65x_{CO_2}^{1.0134}) \quad (2)$$

56 322 where  $\mu_s$  in [Pa·s] is the viscosity of dead water as a function of pressure and temperature,  
 57 323 and  $x_{CO_2}$  is the mass fraction of dissolved CO<sub>2</sub> at experimental conditions. Due to the lack of  
 58 324 published measurements of  $\mu_s$  for all tested salt types and temperatures of our dead solutions,



325 we adopted the approach of Saunders et al. [55] to infer the dead water viscosity from the  
1 326 measured electrical conductivity. The calculated values of  $\mu_s$  for our dead solutions were  
2 327 compared against available published data (for the same salts at concentrations and  
3 328 temperatures consistent with our experimental conditions), and the discrepancy was found to  
4 329 be less than 2% thus confirming the appropriateness of the approach.

6 330 The mass fraction of dissolved  $\text{CO}_2$  ( $x\text{CO}_2$ ) was evaluated using the model of Zhao et al.  
7 331 [57,58] and validated for 0.05M NaCl live water against the experimental values reported by  
8 332 Islam and Carlson [56] for 40°C and 7.5 MPa, and was found to be identical within 1%  
9 333 discrepancy.

12 334 The exponent in **Eq.2** was assumed to be constant for all types of live water investigated here,  
13 335 since it only defines how the solubility of  $\text{CO}_2$  depends on the salt type, and the solubility was  
14 336 reported to be nearly identical for all tested salts at ionic strength of 0.05M (e.g., [59]).

### 16 337 **3. Results and discussion**

#### 18 338 **3.1. Streaming potential coupling coefficient measurements**

20 339 Typical results of PS experiments for select experimental conditions are shown in **Figure 2**.  
21 340 The noise level of the stabilized voltage measured for live water (**Fig. 2c**) was considerably  
22 341 higher than for dead water (**Fig. 2a**). Moreover, the static voltage (i.e., the voltage that  
23 342 corresponds to no-flow conditions and zero pressure difference across the sample) measured  
24 343 for live water did not always return to the exact initial value (as prior to the core flooding  
25 344 experiment), thus contributing to additional error in the streaming potential coupling coefficient  
26 345 and the corresponding zeta potential.

28 346 Experimental repeatability at a given flow rate with live water was also poorer when compared  
29 347 with dead water (compare the scatter for a given pressure difference in **Figs. 2b** and **2d**). The  
30 348 values of all measured streaming potential coupling coefficients inclusive of all experimental  
31 349 uncertainties (obtained from the variation in the slope of the linear regression within the error  
32 350 bars that account for the noise level and repeatability, as shown in **Fig. 2b** and **2d**) are  
34 351 summarized in **Table 3**.

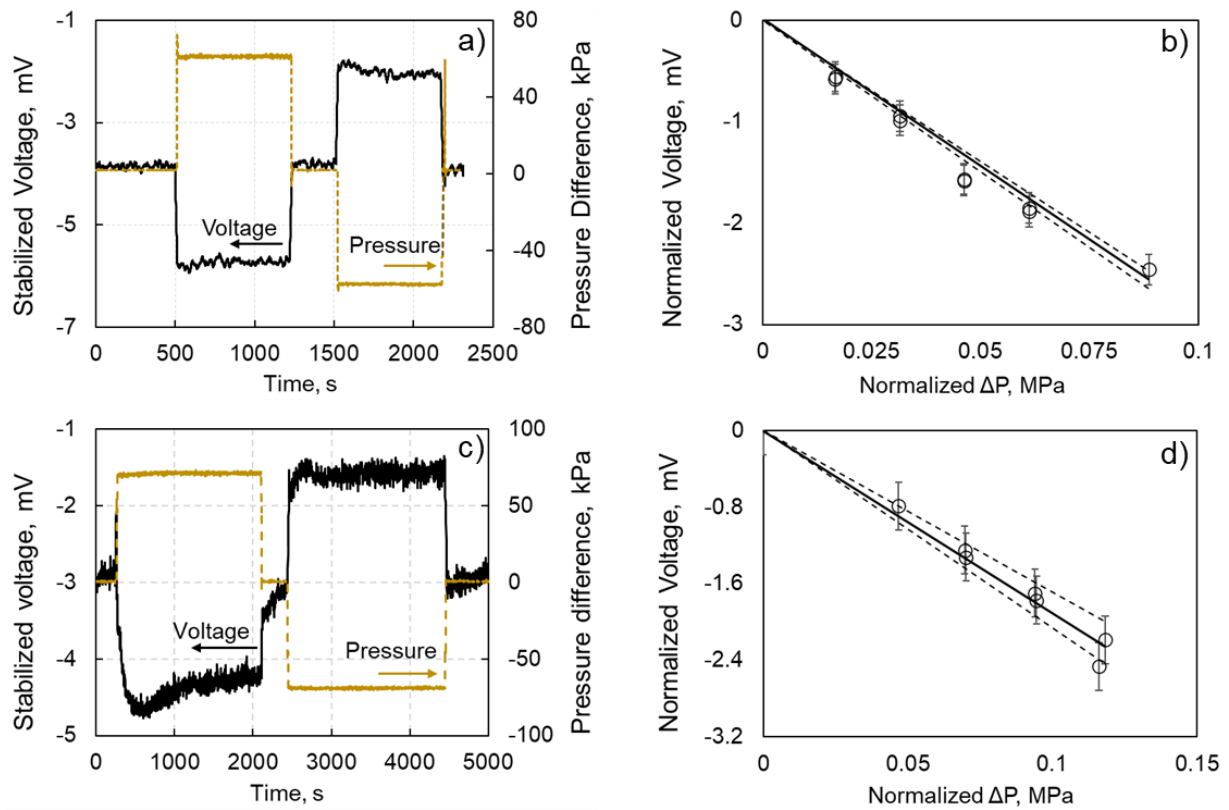


**Figure 2.** Typical results of paired stabilized (PS) experiments (a, c) and the streaming potential coupling coefficient represented by the linear slope of the stabilized voltage,  $\Delta V$ , plotted against the stabilized pressure difference,  $\Delta P$  (b, d). (a) dead NaCl solution pumped at a constant rate of 4 ml/min, temperature of 23°C and pore pressure of 7.5 MPa; (b)  $C_{SP}$  interpreted from the data of (a); (c) typical data of PS experiment carried out with live NaCl solution at constant rate of 6 ml/min, temperature of 40°C, pressure of 7.5 MPa; (d)  $C_{SP}$  interpreted from the data of (c). Dashed lines represent possible variation of  $C_{SP}$  within the total experimental uncertainty denoted by the error bars.

### 3.2. Dead water zeta potential

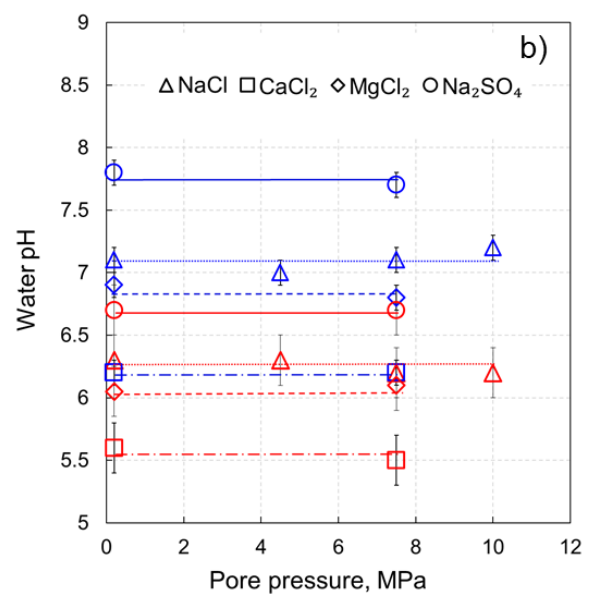
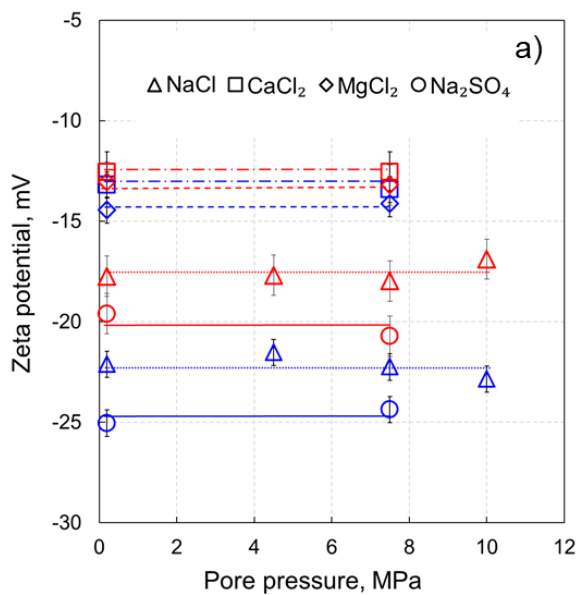
Zeta potentials for dead water remained negative for all tested conditions. Moreover, for any given temperature and salt type, the zeta potential was independent of the pore pressure (Figure 3a). Dead water equilibrium pH values were also independent of pore pressure for any given salt type (Fig.3b), which implied that the amount of dissolved  $\text{CO}_2$  remained constant during the experiments. However, pH decreased with increasing temperature, consistent with previously reported studies [16,40,60,61].

The largest in magnitude zeta potential was obtained with  $\text{Na}_2\text{SO}_4$ , and it became progressively smaller in magnitude when using NaCl,  $\text{MgCl}_2$  and  $\text{CaCl}_2$ , ( $|\zeta_{\text{Na}_2\text{SO}_4}| > |\zeta_{\text{NaCl}}| > |\zeta_{\text{MgCl}_2}| > |\zeta_{\text{CaCl}_2}|$ ). A difference of less than 1 mV between the zeta potentials of  $\text{MgCl}_2$  and  $\text{CaCl}_2$  was observed for both salts at both temperatures of 23°C and 40°C. Although this difference was small, it was comparable to the difference of 2mV reported by Vinogradov et al. [40] for the same salt types. The measured pH of solutions in contact with the sample became smaller with the transition from  $\text{Na}_2\text{SO}_4$  to NaCl, followed by  $\text{MgCl}_2$  and  $\text{CaCl}_2$  ( $\text{pH}_{\text{Na}_2\text{SO}_4} > \text{pH}_{\text{NaCl}} > \text{pH}_{\text{MgCl}_2} > \text{pH}_{\text{CaCl}_2}$ ), qualitatively consistent with previously published studies [40,62].

Water	Pressure, MPa	Temperature, °C	Condition	$C_{SP}$ , mV/MPa
-------	---------------	-----------------	-----------	-------------------

NaCl	0.2	23	Dead water	$-29.9 \pm 0.07$
	4.5	23	Dead water	$-29.9 \pm 0.07$
	7.5	23	Dead water	$-29.9 \pm 0.07$
	10.0	23	Dead water	$-30.7 \pm 0.07$
	0.2	40	Dead water	$-28.8 \pm 0.10$
	4.5	40	Dead water	$-28.3 \pm 0.10$
	7.5	40	Dead water	$-28.5 \pm 0.10$
	10.0	40	Dead water	$-28.3 \pm 0.10$
	4.5	40	Live water	$-23.6^{+1.20}_{-1.30}$
	7.5	40	Live water	$-19.0^{+2.00}_{-1.60}$
10.0	40	Live water	$-18.1^{+1.80}_{-0.70}$	
CaCl <sub>2</sub>	0.2	23	Dead water	$-26.5 \pm 0.07$
	7.5	23	Dead water	$-26.9 \pm 0.07$
	0.2	40	Dead water	$-25.3 \pm 0.10$
	7.5	40	Dead water	$-25.4 \pm 0.10$
	7.5	40	Live water	$-17.6^{+0.90}_{-1.20}$
MgCl <sub>2</sub>	0.2	23	Dead water	$-28.0 \pm 0.07$
	7.5	23	Dead water	$-28.4 \pm 0.07$
	0.2	40	Dead water	$-27.4 \pm 0.07$
	7.5	40	Dead water	$-27.3 \pm 0.07$
	7.5	40	Live water	$-17.8^{+1.40}_{-1.00}$
Na <sub>2</sub> SO <sub>4</sub>	0.2	23	Dead water	$-56.4 \pm 0.12$
	7.5	23	Dead water	$-55.6 \pm 0.12$
	0.2	40	Dead water	$-44.8 \pm 0.20$
	7.5	40	Dead water	$-43.1 \pm 0.20$
	7.5	40	Live water	$-24.1^{+1.20}_{-2.20}$

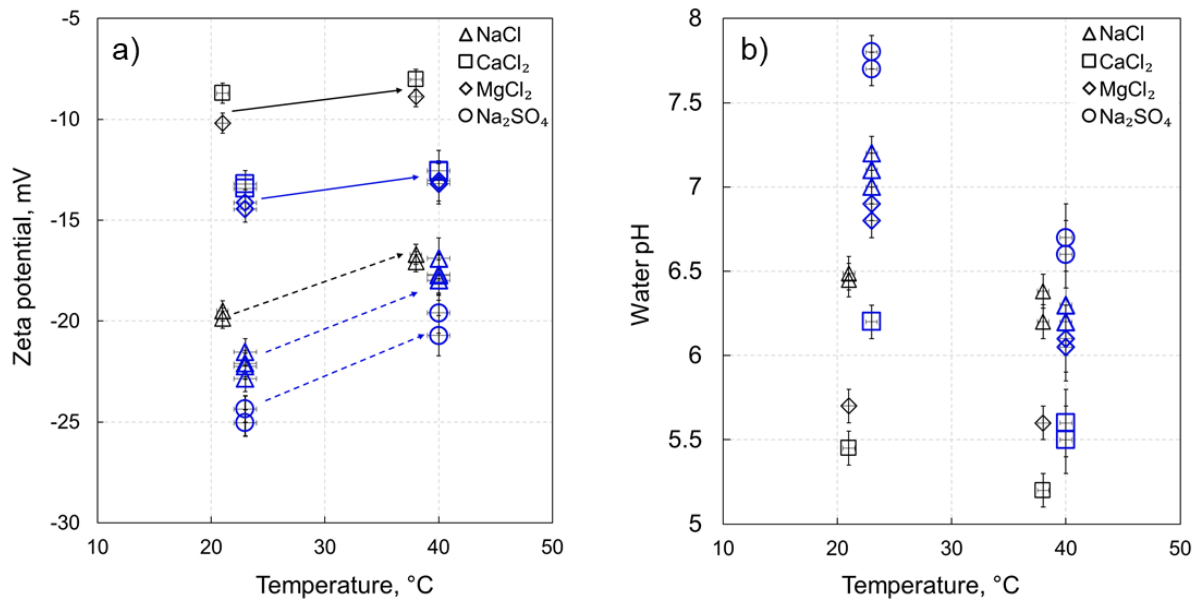
**Table 3.** Streaming potential coupling coefficient ( $C_{SP}$ ) measured for all tested experimental conditions. The ionic strength of all solution was kept constant at 0.05 M. The reported uncertainties in the table are based on both noise level and repeatability, both of which results in linear regressions slope variation as shown in **Fig.2b** and **Fig.2d**.



381

382 **Figure 3.** Zeta potential a) and pH values b) as a function of pore pressure for all dead water  
 1 383 experiments. Blue symbols denote experiments conducted at 23°C; red symbols denote experiments  
 2 384 conducted at 40°C.

385 To quantify the effect of salt type and temperature, zeta potential and water pH were plotted  
 5 386 versus temperature (**Figure 4**). The zeta potential became more positive with increasing  
 6 387 temperature, while water pH decreased with increasing temperature, consistent with  
 7 388 previously published results [16,40]. The highest rate of increase in the zeta potential with  
 8 389 temperature was observed for NaCl (a change of +4.3 mV when transitioning from 23°C to  
 9 390 40°C). An increase in zeta potential (+4.3 mV) was also observed for Na<sub>2</sub>SO<sub>4</sub> when  
 11 391 temperature increased from 23°C to 40°C. In contrast, zeta potential increased with increasing  
 12 392 temperature by 1.0 mV for both, CaCl<sub>2</sub> and MgCl<sub>2</sub>, when temperature increased from 23°C to  
 13 393 40°C. Therefore, a weaker temperature dependence of the zeta potential was observed for  
 14 394 CaCl<sub>2</sub> and MgCl<sub>2</sub>, again consistent with Vinogradov et al. [40].



395 **Figure 4.** Zeta potential a) and pH values b) as a function of temperature for all tested dead water  
 396 experiments. The data for NaCl, CaCl<sub>2</sub>, MgCl<sub>2</sub> and Na<sub>2</sub>SO<sub>4</sub> obtained in this work are shown in blue. Also  
 397 shown for comparison are the data in black obtained with Fontainebleau sandpacks saturated with  
 398 0.015 M solution NaCl, CaCl<sub>2</sub> and MgCl<sub>2</sub> reported by Vinogradov et al. [40].

400 However, the rate of pH change with temperature was higher when compared to Vinogradov  
 401 et al. [40]. Moreover, the pH values measured in our experiments were generally larger than  
 402 those in Vinogradov et al. [40] for the same salt type at any given temperature. The ionic  
 403 strength used by Vinogradov et al. [40] was 0.015 M, which is more than three-fold lower than  
 404 that tested in this study, hence their zeta potentials at lower salinity were expected to be larger  
 405 in magnitude compared to ours. Since the zeta potentials reported by Vinogradov et al. [40]  
 406 were smaller in magnitude compared with our results, we believe that their pH values were  
 407 correct, although different from ours, and had stronger effect on the zeta potential than salinity.

408 Our results suggest that temperature and salt type affect the pH, which in turn affects the  
 409 magnitude of the zeta potential of sandstones saturated with dead water (Figure 5). Based on  
 410 the results for dead water we propose two distinct linear correlations:

$$\zeta_M [mV] = -4.86 \times pH + 12.57; R^2 = 0.976 \quad (3)$$

$$\zeta_D [mV] = -1.35 \times pH - 4.96; R^2 = 0.973 \quad (4)$$

Where  $\zeta_M$  and  $\zeta_D$  denote the zeta potential for water containing monovalent ( $\text{Na}^+$ ) or divalent ( $\text{Ca}^{2+}$  and/or  $\text{Mg}^{2+}$ ) cations, respectively. Regardless of anion type ( $\text{Cl}^-$  or  $\text{SO}_4^{2-}$ ) all experimental points for  $\text{Na}^+$  containing solutions align on the same trendline, and so do the points for all  $\text{CaCl}_2$  and  $\text{MgCl}_2$  experiments regardless of the cation type (**Fig. 5**).

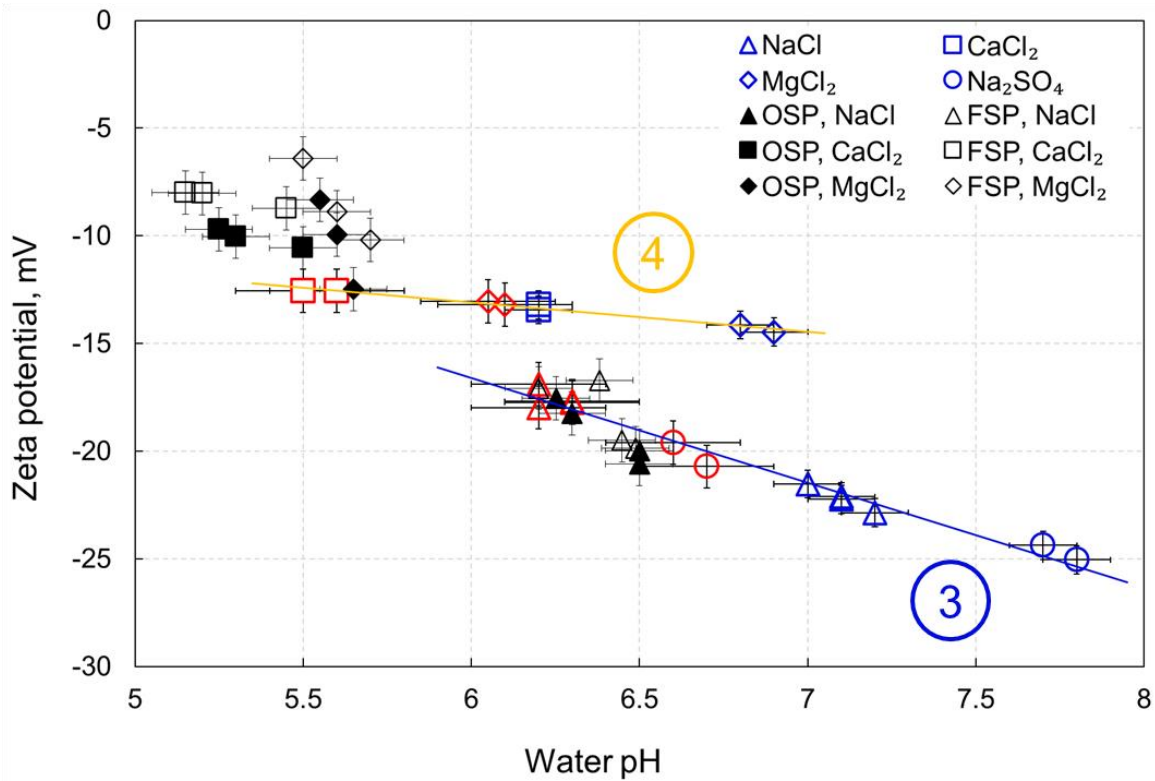


**Figure 5.** Zeta potential as a function of dead water pH for different salt types. Our data are shown in colored symbols; literature data are shown in black [40] and corresponds to Ottawa (OSP) and Fontainebleau (FSP) sandpacks (both >99 wt% quartz content) saturated with 0.015 M dead water. Blue symbols correspond to 23°C, red symbols correspond to 40°C. The blue trendline indicates the linear relationship between the zeta potential of  $\text{Na}^+$  containing salts ( $\text{NaCl}$ ,  $\text{Na}_2\text{SO}_4$ ) and pH (**Eq.3**). The yellow trendline indicates the linear correlation between zeta potential and pH of dead  $\text{CaCl}_2$  and  $\text{MgCl}_2$  solutions (**Eq.4**).

The trend obtained for  $\text{Na}^+$  solutions (**Eq.3**) is identical to that reported for zeta potentials of sandpacks [40]. However, as seen in **Figure 5** the zeta potentials at 23°C measured in this work (blue triangles) were more negative compared with values of Vinogradov et al. [40] and corresponded to higher pH values. The values that correspond to 40°C were consistent with those reported by Vinogradov et al. [40] thus implying stronger temperature effect on both pH and zeta potentials.

In contrast, the trend for divalent cations (**Eq.4**) had a flatter slope, compared with that of **Eq.3**. Such flattening of the slope is consistent with the pH dependence of  $\text{CaCl}_2$  solution relative to that of  $\text{NaCl}$  proposed by Vinogradov et al. [40]. Overall, however, all our  $\zeta_D$  were more negative than those reported by Vinogradov et al. [40], except for the value at pH = 5.7.

The effect of temperature on pH of divalent solutions ( $\text{CaCl}_2$ ,  $\text{MgCl}_2$ ), denoted by the shift from blue to red symbols in **Fig.5**, was substantially more pronounced in this work compared to Vinogradov, et al. [40]. Moreover, Vinogradov et al. [40] also suggested that the response of  $\zeta_D$  to varying pH of  $\text{CaCl}_2$  solution was different to that of  $\text{MgCl}_2$ , and they attributed this difference to a higher activity of  $\text{Mg}^{2+}$  towards the mineral surface compared with  $\text{Ca}^{2+}$  at

438 elevated temperature, i.e. fully hydrated  $Mg^{2+}$  at ambient temperature has larger diameter than  
439  $Ca^{2+}$  making the latter to be closer to the mineral surface and thus more active [62], but at  
440 higher temperatures it becomes smaller by losing hydration shells at a higher rate, approaches  
441 the mineral surface closer and becomes more active. We did not observe any difference in  
442 response of  $\zeta_D$  to varying pH of either solution at elevated temperature, but we only  
443 investigated temperatures of 23°C and 40°C whilst the data presented by Vinogradov et al.  
444 [40] included experiments conducted at 70°C and 120°C where the split in response of  $\zeta_D$  to  
445 pH for  $CaCl_2$  and  $MgCl_2$  was observed. Using **Eqs.3** and **4** allows to accurately predict the  
446 expected zeta potential as a function of pH for single salt electrolytes. However, additional  
447 work is required to investigate whether the proposed trends can be interpolated for mixtures  
448 of different salts.

449 To validate the proposed correlations between water pH and the zeta potential (**Eqs.3-4**) we  
450 compared the values computed using these equations against previously published  
451 experimental data. Walker and Glover [32] obtained over 100 zeta potential measurements  
452 on intact Fontainebleau sample (F3Q) at 23°C at reported pH of 6.48 and ambient pressure  
453 (i.e., atmospheric content of dissolved  $CO_2$ , hence dead water). From the entire NaCl salinity  
454 range tested by Walker and Glover [32], the closest to the ionic strength tested in this study  
455 was 0.062 M, for which Walker and Glover [32] reported the measured zeta potential of -  
456  $18 \pm 1$  mV. Using **Eq.3** and pH of 6.48 [32] the calculated  $\zeta_M = -18.92$  mV, which lies within the  
457 experimental uncertainty and consistent with the value of -18 mV predicted by the pH  
458 dependence of the zeta potential model [63].

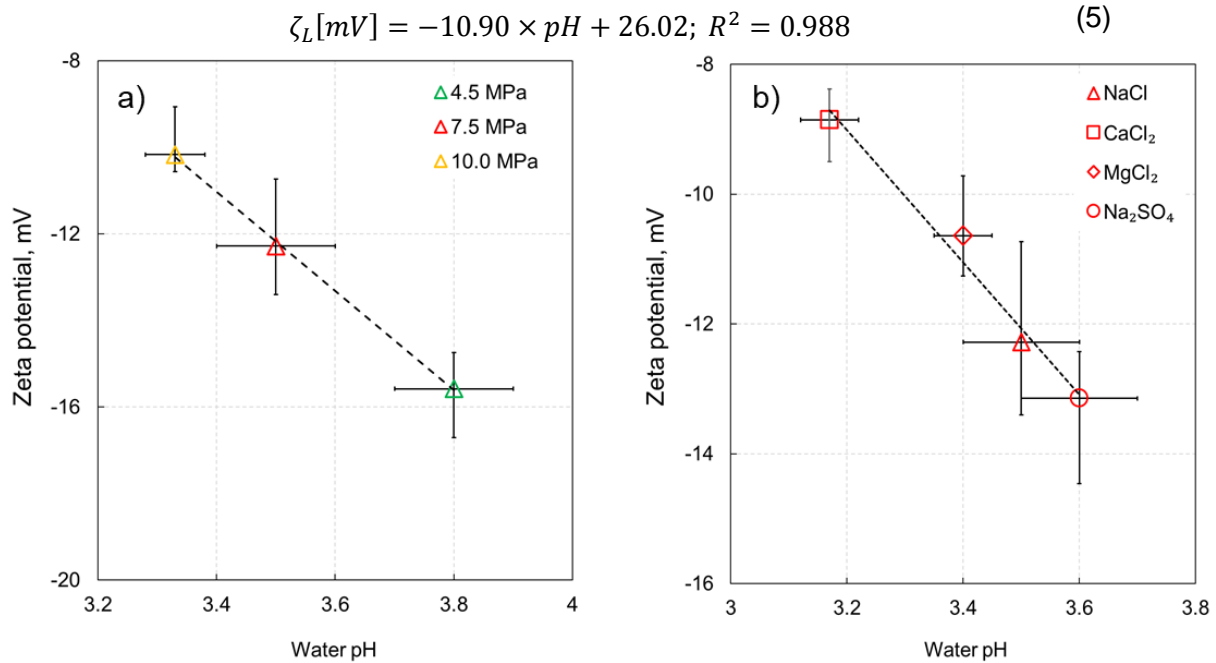
459 Another study that reported measurements of the zeta potential in intact sandstone samples  
460 saturated with 0.01 M dead NaCl was published by Vinogradov and Jackson [16]. In that study  
461 the authors reported pH of  $6.75 \pm 0.03$  measured in experiments with St Bees1, St Bees 2,  
462 Doddington and Stainton samples at  $22 \pm 1^\circ C$ . For all four sandstone samples saturated with  
463 0.01 M dead NaCl at ambient pressure the reported zeta potential was  $-22 \pm 0.4$  mV. Using our  
464 regression for pH dependence of the zeta potential defined by **Eq.3**, the estimated value was  
465 found to be -20.24 mV thus validating our approach.

466 To confirm our proposed model for  $\zeta_D$  obtained with dead solutions, we compared predictions  
467 on the zeta potential made using **Eq.4** against published experimental data [64] obtained with  
468 Berea sandstone saturated with  $10^{-3}$  M  $CaCl_2$  and  $MgCl_2$  solutions at pH between 6.0 and 7.5.  
469 Our model yields  $\zeta_D$  for both solutions between -13.06 mV and -15.09 mV (depending on the  
470 used pH value) compared with -9.3 mV and -6.6 mV reported by Thanh and Sprik [64] for  
471  $MgCl_2$  and  $CaCl_2$ , respectively. The values obtained using **Eq.4** are more negative in  
472 comparison to those measured by Thanh and Sprik [64] and we attribute this difference to  
473 presence of clay minerals in the work of Thanh and Sprik [64], which are known to be more  
474 reactive towards divalent cations. On the other hand, the zeta potential reported in the same  
475 paper for  $10^{-3}$  M NaCl and  $Na_2SO_4$  at pH between 6.0 and 7.5 was also compared against our  
476 model (**Eq.3**). Our prediction for  $\zeta_M$  was found to be in the range between -16.59 mV and -  
477 23.88 mV (corresponding to pH range), which is in a good agreement with the reported by  
478 Thanh and Sprik [64] values of -23.9 mV and 24.4 mV for NaCl and  $Na_2SO_4$ , respectively.

### 479 **3.3. Live water zeta potential**

480 Due to initial mixing of 400 mL of live water with 30 mL of dead water, the resulting pH of all  
481 re-equilibrated solutions in this study were approximately 0.8 pH units higher than those  
482 measured by Li et al. [65] and Peng et al. [47] for the same pressure.

483 Increasing pore pressure resulted in increased CO<sub>2</sub> dissolution and formation of carbonic acid,  
 1 484 and thus a decreasing water pH and consequently a more positive zeta potential (**Fig.6a**). All  
 2 485 three zeta potentials measured with NaCl at 4.5 MPa, 7.5 MPa and 10 MPa linearly correlated  
 3 486 with the corresponding water pH, with the slope of the linear regression (**Eq.5**), which was  
 4 487 significantly different from that obtained with dead Na<sup>+</sup> containing solutions (**Eq.3**).  
 5 488 Furthermore, all four salt types tested at 7.5 MPa lied on a linear trendline (**Fig.6b**), with the  
 6 489 slope consistent with that of **Fig.6a**:



491 **Figure 6.** Zeta potential as a function of live water pH for a) NaCl solutions (with varying pore pressure  
 492 and therefore different amount of dissolved CO<sub>2</sub>) and b) all salt types at pore pressure of 7.5 MPa. All  
 493 data were measured at 40°C. The linear regressions in both figures correspond to **Eq. 5**.

494 A summary plot including both, dead and live water solutions, is presented in **Figure 7**, which  
 495 suggests that either: a) **Eq.4** should be used for both dead and live CaCl<sub>2</sub>/MgCl<sub>2</sub> solutions,  
 496 while **Eq.3** should be used for dead NaCl/Na<sub>2</sub>SO<sub>4</sub> and **Eq.5** should be used for live  
 497 NaCl/Na<sub>2</sub>SO<sub>4</sub> solutions; or alternatively b) **Eq.5** should be used for all types of live solutions  
 498 (green regression in **Fig.7**) while **Eq.3** and **Eq.4** should be used for dead NaCl/Na<sub>2</sub>SO<sub>4</sub> and  
 499 CaCl<sub>2</sub>/MgCl<sub>2</sub> solutions, respectively.

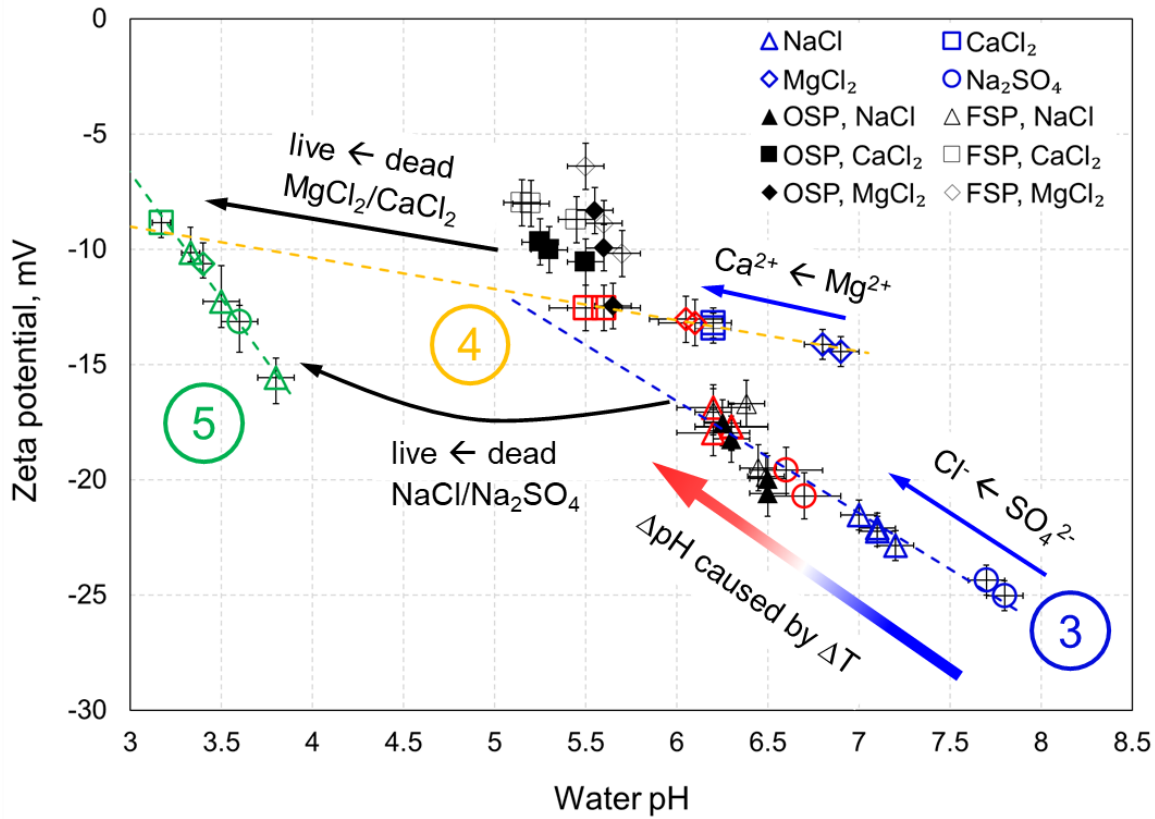


**Figure 7.** Zeta potentials measured versus pH of dead and live aqueous solutions. Our data across all pore pressures, temperatures and salt types are shown in color. Literature data for Ottawa and Fontainebleau sandpacks (OSP and FSP, respectively) saturated with 0.015 M dead water [40] are shown in black. The blue and red symbols correspond to 23°C and 40°C, respectively. The blue and yellow trendlines are the same as in Fig.5 and correspond to Eq.3 and Eq.4, respectively. The green trendline is identified for all dead water data and given by Eq.5. The arrows are added to explain the mechanisms of the zeta potential variation along and/or between the trendlines.

All of the regressions proposed here for dead and live water solutions (Eq.3-5) appear to have a non-zero intercept with the horizontal axis, which is defined as the Isoelectric Point (IEP) that identifies the value of pH that results in a zero zeta potential. For the experiments with dead NaCl and Na<sub>2</sub>SO<sub>4</sub> solutions, the IEP is calculated using Eq.3 and equals 2.59, while the corresponding value for all live water solution calculated using Eq.5 is 2.39. Both values are consistent with a published study that reported IEP for quartz and NaCl to be in the range between pH2.2 and pH2.5 [48]. However, the IEP found for CaCl<sub>2</sub> and MgCl<sub>2</sub> (Eq.4) appears to be at pH of -3.67, which is inconsistent with all previously published results. Therefore, we hypothesize that the regression for pH dependence of the zeta potential with divalent cation salts is not linear throughout the entire range of pH and changes slope at pH around 3.3 where the regression defined by Eq.4 intersects with the regression given by Eq.5. This hypothesis is consistent with our results for Na<sup>+</sup> containing solution that appear to switch from the pH dependence defined by Eq.3 to that given by Eq.5. Moreover, a published experimental study [66] on crushed Fontainebleau samples saturated with NaCl of resistivity of 100 Ω·m (equivalent to ionic strength of 10<sup>-3</sup> M) demonstrated that pH dependence of the zeta potential was non-uniform. The rate of increase of the measured by Lorne et al. [66] zeta potential with decreasing pH was nearly linear but became significantly steeper below c. pH = 3.5 and had IEP at pH2.5, so that both observations are consistent with our results.

To confirm the pH dependence of  $\zeta_M$ ,  $\zeta_D$  and  $\zeta_L$  across the entire pH range, additional experiments at pore pressures that correspond to pH between 4 and 6 for Na<sup>+</sup> containing



528 solutions, and between pH3.5 and pH5.5 for CaCl<sub>2</sub> and MgCl<sub>2</sub> are required to cover the  
1 529 intermediate pH range. Moreover, additional experiments are also required for all types of  
2 530 solutions at pore pressures that correspond to pH<3.2 (i.e., higher partial CO<sub>2</sub> pressure) to  
3 531 investigate the pH dependence of  $\zeta_M$  and  $\zeta_D$  under these live water conditions.

#### 5 532 **4. Implications for CO<sub>2</sub> geological storage**

7 533 The empirical trends for the zeta potential as a function of water pH (**Eqs.3-5**) proposed in this  
8 534 study bear a significant scientific and technological value as they can be used for predicting  
9 535 the expected zeta potential for shallow subsurface settings (low pressure and hence dead  
10 536 water-like behavior of the fluid), as well as for deep formations characterized by high content  
11 537 of dissolved CO<sub>2</sub> (live water-like behavior of the fluid). From the proposed correlations the  
12 538 streaming potential coupling coefficient can be interpreted using Helmholtz-Smoluchowski  
13 539 equation and used for monitoring and characterizing subsurface flows of injected CO<sub>2</sub> or  
14 540 carbonated water during CGS [38]. Moreover, the correlations are important when applied to  
15 541 monitoring movement of water in subsurface settings characterized by variable pH such as  
16 542 hydrocarbon reservoirs (e.g., [15]), groundwater [67, 68] or geothermal [69] systems. Our  
17 543 results demonstrate that temperature does not directly affect the zeta potential, instead it  
18 544 affects solubility of CO<sub>2</sub> and pH of aqueous solutions, which in turn impacts the zeta potential.  
19 545 In this sense, laboratory measurements of natural water pH or under varying temperature and  
20 546 CO<sub>2</sub> pressure can be acquired and zeta potential interpreted from the measured values using  
21 547 **Eq.3-5**.

26 548 Moreover, the proposed empirical correlations for the mineral-water zeta potential can be  
27 549 incorporated in the classical DLVO theory (e.g., [43]) to yield system's wettability thus  
28 550 quantifying the potential of residual trapping of CO<sub>2</sub> during geological sequestration in  
29 551 sandstone formations. For instance, our results suggest that higher reservoir pressure that  
30 552 corresponds to enhanced CO<sub>2</sub> dissolution will result in lower pH and smaller in magnitude  
31 553 rock-water zeta potential thus implying a smaller electrostatic component of the disjoining  
32 554 pressure and hence, less water-wet conditions. In such case, pure sandstone reservoirs  
33 555 (>95% quartz) might be deemed inappropriate for CO<sub>2</sub> injection for geological storage and  
34 556 other formations containing more clays, which are known to make zeta potential larger in  
35 557 magnitude (compare the reported zeta potential measured on Buff Berea, Grey Berea and  
36 558 Parker sandstones saturated with 0.5% NaCl, CaCl<sub>2</sub> and MgCl<sub>2</sub> in Shehata and Nasr-El-Din  
37 559 [70], to be considered. On the other hand, our results suggest that residual CO<sub>2</sub> trapping  
38 560 controlled by wettability can potentially be improved by making the rock more water-wet via  
39 561 injection of NaCl or Na<sub>2</sub>SO<sub>4</sub> rich water of low salinity prior to injecting CO<sub>2</sub> for geological  
40 562 storage. Such procedure would lead to a larger in magnitude negative zeta potential at rock-  
41 563 water interface, so that the shift towards more water-wet conditions would occur assuming  
42 564 that the zeta potential at CO<sub>2</sub>-water interface is also negative.

47 565 Furthermore, higher CO<sub>2</sub> pressure, and therefore, higher dissolved CO<sub>2</sub> concentration, causes  
48 566 the equilibrium pH to decrease thus also affecting the mineralization of carbonate and  
49 567 therefore, the CO<sub>2</sub> ultimate storage capacity [71–73].

51 568 Despite the fact that our results have been able thus far to accurately predict zeta potential  
52 569 under ambient and supercritical CO<sub>2</sub> conditions, additional experiments are required to  
53 570 quantify the pH dependence of the zeta potential for intermediate pH range of 4.0-5.5 for all  
54 571 types of salts. Additional work is also required to test the pH dependence of the zeta potential  
55 572 for pH<3, for mixtures of salts to replicate complex natural aqueous solutions that saturate  
56 573 geological porous media, as well as for higher ionic strength solutions typically found in deep  
57 574 sandstone formations such as deep saline aquifers or depleted hydrocarbon reservoirs.

## 575 5. Conclusions

1  
2 576 We have developed the experimental methodology and for the first time successfully carried  
3 577 out the streaming potential measurements in intact sandstone sample saturated with CO<sub>2</sub>-rich  
4 578 aqueous solutions of 0.05 M ionic strength under high pressure (up to 10 MPa) and elevated  
5 579 temperature (up to 40°C) conditions. For the first time, all streaming potential measurements  
6 580 on silica in contact with aqueous solutions fully equilibrated with CO<sub>2</sub> (live water experiments)  
7 581 were obtained at equilibrium conditions of pressure and temperature that correspond to CO<sub>2</sub>  
8 582 at supercritical state. The zeta potential was carefully interpreted from the measurements and  
9 583 we found that:

- 12 584 1. The zeta potential for all tested solutions, pressure and temperature was negative,  
13 585 which implied that the electrical charge at rock-water interface was always negative  
14 586 and non-zero.
- 16 587 2. The zeta potential of all dead solutions was found to be independent of pore pressure  
17 588 but decreased with increasing temperature; this finding is consistent with previously  
18 589 published data obtained at ambient pressure [40].
- 19 590 3. The zeta potential of all dead solutions was found to be different for NaCl/Na<sub>2</sub>SO<sub>4</sub>  
20 591 compared with that of CaCl<sub>2</sub>/MgCl<sub>2</sub>.; the finding for Na<sub>2</sub>SO<sub>4</sub> is new but the observation  
21 592 for NaCl vs CaCl<sub>2</sub>/MgCl<sub>2</sub> is consistent with the reported results [40].
- 23 593 4. The negative zeta potential of all live solutions decreased in magnitude with increasing  
24 594 pore pressure, reflecting the effect of enhanced CO<sub>2</sub> dissolution under high pressure,  
25 595 which caused pH to decrease; the effect of CO<sub>2</sub> dissolution on the zeta potential has  
26 596 been quantified for the first time in this study.
- 28 597 5. Our results indicate that pH of dead and live solutions is the only control of the zeta  
29 598 potential so that salt type, pore pressure and temperature indirectly affect it via having  
30 599 an impact on pH.
- 31 600 6. We proposed three linear empirical correlations with a high coefficient of determination  
32 601 ( $R^2 > 0.97$ ) to predict the zeta potentials as a function of water pH. The correlations  
33 602 reflect a different response of the zeta potential to presence of mono- or divalent  
34 603 cations in dead solutions, and a distinctly different response to the live water  
35 604 conditions. The correlation for the live water is the first of a kind, thus providing a good  
36 605 source for validating surface complexation models for silica in contact with carbonated  
37 606 aqueous solutions at supercritical CO<sub>2</sub> conditions.
- 40 607 7. The proposed correlations were validated against published experimental data and  
41 608 were confirmed to accurately predict the zeta potential of dead solutions. The iso-  
42 609 electric point predicated by our live water correlation was found to be similar to that  
43 610 published for dead water solutions [48].
- 44 611 8. Our novel results have significant implications for many subsurface settings where high  
45 612 concentration of dissolved CO<sub>2</sub> is expected. Potential applications include  
46 613 management of aquifers, geothermal sources and CGS. Moreover, an improved  
47 614 understanding of the zeta potential of silica-water systems under supercritical CO<sub>2</sub>  
48 615 conditions resulting from this study will inform future studies on thermodynamics of  
49 616 wettability [43], colloid stability and use of nanoparticles [74].

52 617 Future experimental work will aim at acquiring zeta potential values in systems comprising  
53 618 clayey sandstones, CO<sub>2</sub>-rich aqueous solutions with pH between 4.0 and 5.5, CO<sub>2</sub> pressure  
54 619 higher than 10 MPa that corresponds to pH below 3, ionic strength higher than 0.1 M, and  
55 620 complex background solutions. Moreover, the planned experimental work will investigate  
56 621 impact of grain size, shape, packing and roughness on the zeta potential as well as alternative  
57 622 experimental methods [75]. These experiments will complement the data reported here and

623 expand the range of tested conditions not covered in this work, thus further improving our  
1 624 understanding of the zeta potential at the silica-water interfaces under conditions relevant to  
2 625 CGS. The results will also be used to inform future surface complexation and molecular  
3 626 dynamics simulation studies aimed at describing silica-water-CO<sub>2</sub> systems under CSG  
4 627 conditions.  
5

## 6 628 **Acknowledgements**

8 629 Miftah Hidayat was supported by the Aberdeen-Curtin PhD studentship. David Vega-Maza is  
9 630 funded by the Spanish Ministry of Science, Innovation and Universities (“Beatriz Galindo  
10 631 Senior” fellowship BEAGAL18/00259). The authors would also like to thank the Edith Cowan  
11 632 University for funding the design, manufacturing and testing of the experimental setup through  
12 633 RG14747 research grant awarded to the University of Aberdeen.  
13  
14

15 634  
16  
17  
18  
19  
20  
21  
22  
23  
24  
25  
26  
27  
28  
29  
30  
31  
32  
33  
34  
35  
36  
37  
38  
39  
40  
41  
42  
43  
44  
45  
46  
47  
48  
49  
50  
51  
52  
53  
54  
55  
56  
57  
58  
59  
60  
61  
62  
63  
64  
65

635 **References**

- 1  
2 636 [1] A.B. Ronov, A.A. Yaroshevsky, Chemical Composition of the Earth's Crust, Earth's  
3 637 Crust Up. Mantle. (1969) 37–57. <https://doi.org/10.1029/GM013p0037>.
- 4 638 [2] W.M. Edmunds, P.L. Smedley, Residence time indicators in groundwater: the East  
5 639 Midlands Triassic sandstone aquifer, Appl. Geochemistry. 15 (2000) 737–752.  
6 640 [https://doi.org/10.1016/S0883-2927\(99\)00079-7](https://doi.org/10.1016/S0883-2927(99)00079-7).
- 7 641 [3] W.M. Edmunds, A.H. Bath, D.L. Miles, Hydrochemical evolution of the East Midlands  
8 642 Triassic sandstone aquifer, England, Geochim. Cosmochim. Acta. 46 (1982) 2069–  
9 643 2081. [https://doi.org/10.1016/0016-7037\(82\)90186-7](https://doi.org/10.1016/0016-7037(82)90186-7).
- 10 644 [4] M.R. Coop, S.M. Willson, Behavior of Hydrocarbon Reservoir Sands and Sandstones,  
11 645 J. Geotech. Geoenvironmental Eng. 129 (2003) 1010–1019.  
12 646 [https://doi.org/10.1061/\(ASCE\)1090-0241\(2003\)129:11\(1010\)](https://doi.org/10.1061/(ASCE)1090-0241(2003)129:11(1010)).
- 13 647 [5] M.Y. Gulamali, E. Leinov, M.D. Jackson, Self-potential anomalies induced by water  
14 648 injection into hydrocarbon reservoirs, Geophysics. 76 (2011) F283–F292.  
15 649 <https://doi.org/10.1190/1.3596010>.
- 16 650 [6] L. Aquilina, H. Pauwels, A. Genter, C. Fouillac, Water-rock interaction processes in the  
17 651 Triassic sandstone and the granitic basement of the Rhine Graben: Geochemical  
18 652 investigation of a geothermal reservoir, Geochim. Cosmochim. Acta. 61 (1997) 4281–  
19 653 4295. [https://doi.org/10.1016/S0016-7037\(97\)00243-3](https://doi.org/10.1016/S0016-7037(97)00243-3).
- 20 654 [7] R.B. Schmidt, K. Bucher, K. Drüppel, I. Stober, Experimental interaction of  
21 655 hydrothermal Na-Cl solution with fracture surfaces of geothermal reservoir sandstone  
22 656 of the Upper Rhine Graben, Appl. Geochemistry. 81 (2017) 36–52.  
23 657 <https://doi.org/10.1016/j.apgeochem.2017.03.010>.
- 24 658 [8] W. Daily, A. Ramirez, D. LaBrecque, J. Nitao, Electrical resistivity tomography of  
25 659 vadose water movement, Water Resour. Res. 28 (1992) 1429–1442.  
26 660 <https://doi.org/10.1029/91WR03087>.
- 27 661 [9] R.D. Ogilvy, P.I. Meldrum, O. Kuras, P.B. Wilkinson, J.E. Chambers, M. Sen, A. Pulido-  
28 662 Bosch, J. Gisbert, S. Jorreto, I. Frances, P. Tsourlos, Automated monitoring of coastal  
29 663 aquifers with electrical resistivity tomography, Near Surf. Geophys. 7 (2009) 367–376.  
30 664 <https://doi.org/10.3997/1873-0604.2009027>.
- 31 665 [10] M.W. Haartsen, S.R. Pride, Electro seismic waves from point sources in layered media,  
32 666 J. Geophys. Res. Solid Earth. 102 (1997) 24745–24769.  
33 667 <https://doi.org/10.1029/97JB02936>.
- 34 668 [11] L. Jouniaux, F. Zyserman, A review on electrokinetically induced seismo-electrics,  
35 669 electro-seismics, and seismo-magnetics for Earth sciences, Solid Earth. 7 (2016) 249–  
36 670 284. <https://doi.org/10.5194/se-7-249-2016>.
- 37 671 [12] R. Peng, B. Di, P.W.J. Glover, J. Wei, P. Lorinczi, Z. Liu, H. Li, Seismo-electric  
38 672 conversion in shale: experiment and analytical modelling, Geophys. J. Int. 223 (2020)  
39 673 725–745. <https://doi.org/10.1093/gji/ggaa288>.
- 40 674 [13] L. Jouniaux, A. Maineult, V. Naudet, M. Pessel, P. Sailhac, Review of self-potential  
41 675 methods in hydrogeophysics, Comptes Rendus Geosci. 341 (2009) 928–936.  
42 676 <https://doi.org/10.1016/j.crte.2009.08.008>.
- 43 677 [14] A. Revil, A. Jardani, The Self-Potential Method: Theory and Applications in  
44 678 Environmental Geosciences, Cambridge University Press, Cambridge, 2013.  
45 679 [https://doi.org/DOI: 10.1017/CBO9781139094252](https://doi.org/DOI:10.1017/CBO9781139094252).
- 46 680 [15] M.D. Jackson, M.Y. Gulamali, E. Leinov, J.H. Saunders, J. Vinogradov, Spontaneous

- 681 Potentials in Hydrocarbon Reservoirs During Waterflooding: Application to Water-Front  
1 682 Monitoring, *SPE J.* 17 (2012) 53–69. <https://doi.org/10.2118/135146-PA>.
- 2  
3 683 [16] J. Vinogradov, M.D. Jackson, Zeta potential in intact natural sandstones at elevated  
4 684 temperatures, *Geophys. Res. Lett.* 42 (2015) 6287–6294.  
5 685 <https://doi.org/10.1002/2015GL064795>.
- 6  
7 686 [17] C. Vogt, N. Klitzsch, V. Rath, On self-potential data for estimating permeability in  
8 687 enhanced geothermal systems, *Geothermics.* 51 (2014) 201–213.  
9 688 <https://doi.org/10.1016/j.geothermics.2014.01.008>.
- 10  
11 689 [18] D. Jougnot, D. Roubinet, L. Guarracino, A. Mainault, Modeling Streaming Potential in  
12 690 Porous and Fractured Media, Description and Benefits of the Effective Excess Charge  
13 691 Density Approach., in: A. Biswas, S.P. Sharma (Eds.), *Adv. Model. Interpret. Near Surf.*  
14 692 *Geophys.*, Springer International Publishing, 2020: bll 61–96.  
15 693 [https://doi.org/10.1007/978-3-030-28909-6\\_4](https://doi.org/10.1007/978-3-030-28909-6_4).
- 16  
17 694 [19] R.J. Hunter, *Zeta potential in colloid science: principles and applications*, Academic  
18 695 press, New York, 1981.
- 19  
20 696 [20] A. Revil, P.A. Pezard, P.W.J. Glover, Streaming potential in porous media: 1. Theory  
21 697 of the zeta potential, *J. Geophys. Res. Solid Earth.* 104 (1999) 20021–20031.  
22 698 <https://doi.org/10.1029/1999JB900089>.
- 23  
24 699 [21] H. Collini, S. Li, M.D. Jackson, N. Agenet, B. Rashid, J. Couves, Zeta potential in intact  
25 700 carbonates at reservoir conditions and its impact on oil recovery during controlled  
26 701 salinity waterflooding, *Fuel.* 266 (2020) 116927.  
27 702 <https://doi.org/10.1016/j.fuel.2019.116927>.
- 28  
29 703 [22] C.H. Pentland, R. El-Maghraby, S. Iglauer, M.J. Blunt, Measurements of the capillary  
30 704 trapping of super-critical carbon dioxide in Berea sandstone, *Geophys. Res. Lett.* 38  
31 705 (2011). <https://doi.org/10.1029/2011GL046683>.
- 32  
33 706 [23] D.W. Green, G.P. Willhite, *Enhanced oil recovery*, Henry L. Doherty Memorial Fund of  
34 707 AIME, Society of Petroleum Engineers, Richardson, TX, 1998.
- 35  
36 708 [24] S. Iglauer, M. Ali, A. Keshavarz, Hydrogen Wettability of Sandstone Reservoirs:  
37 709 Implications for Hydrogen Geo-Storage, *Geophys. Res. Lett.* 48 (2021)  
38 710 e2020GL090814. <https://doi.org/10.1029/2020GL090814>.
- 39  
40 711 [25] G.J. Hirasaki, Wettability: Fundamentals and Surface Forces, *SPE Form. Eval.* 6 (1991)  
41 712 217–226. <https://doi.org/10.2118/17367-PA>.
- 42  
43 713 [26] M.D. Jackson, D. Al-Mahrouqi, J. Vinogradov, Zeta potential in oil-water-carbonate  
44 714 systems and its impact on oil recovery during controlled salinity water-flooding, *Sci.*  
45 715 *Rep.* 6 (2016) 1–13. <https://doi.org/10.1038/srep37363>.
- 46  
47 716 [27] J.N. Israelachvili, The nature of van der waals forces, *Contemp. Phys.* 15 (1974) 159–  
48 717 178. <https://doi.org/10.1080/00107517408210785>.
- 49  
50 718 [28] J.H. Adair, E. Suvaci, J. Sindel, *Surface and Colloid Chemistry*, in: K.H.J. Buschow,  
51 719 R.W. Cahn, M.C. Flemings, B. Ilshner, E.J. Kramer, S. Mahajan, P.B.T.-E. of M.S. and  
52 720 T. Veyssi re (Eds.), Elsevier, Oxford, 2001: bll 1–10. <https://doi.org/10.1016/B0-08-043152-6/01622-3>.
- 53  
54 722 [29] R.P. Misra, J.P. de Souza, D. Blankschtein, M.Z. Bazant, Theory of Surface Forces in  
55 723 Multivalent Electrolytes, *Langmuir.* 35 (2019) 11550–11565.  
56 724 <https://doi.org/10.1021/acs.langmuir.9b01110>.
- 57  
58 725 [30] A. V Delgado, F. Gonz lez-Caballero, R.J. Hunter, L.K. Koopal, J. Lyklema,  
59 726 Measurement and interpretation of electrokinetic phenomena, *J. Colloid Interface Sci.*  
60 727 309 (2007) 194–224. <https://doi.org/10.1016/j.jcis.2006.12.075>.

- 728 [31] A. Alroudhan, J. Vinogradov, M.D. Jackson, Zeta potential of intact natural limestone:  
 1 729 Impact of potential-determining ions Ca, Mg and SO<sub>4</sub>, *Colloids Surfaces A*  
 2 730 *Physicochem. Eng. Asp.* 493 (2016) 83–98.  
 3 731 <https://doi.org/10.1016/j.colsurfa.2015.11.068>.  
 4
- 5 732 [32] E. Walker, P.W.J. Glover, Measurements of the Relationship Between Microstructure,  
 6 733 pH, and the Streaming and Zeta Potentials of Sandstones, *Transp. Porous Media.* 121  
 7 734 (2018) 183–206. <https://doi.org/10.1007/s11242-017-0954-5>.  
 8
- 9 735 [33] E. Walker, P.W.J. Glover, J. Ruel, A transient method for measuring the DC streaming  
 10 736 potential coefficient of porous and fractured rocks, *J. Geophys. Res. Solid Earth.* 119  
 11 737 (2014) 957–970. <https://doi.org/10.1002/2013JB010579>.  
 12
- 13 738 [34] J. Vinogradov, M.Z. Jaafar, M.D. Jackson, Measurement of streaming potential  
 14 739 coupling coefficient in sandstones saturated with natural and artificial brines at high  
 15 740 salinity, *J. Geophys. Res. Solid Earth.* 115 (2010).  
 16 741 <https://doi.org/10.1029/2010JB007593>.  
 17
- 18 742 [35] H. Collini, M. Jackson, Zeta Potential of the Crude Oil-Brine Interface and Implications  
 19 743 for Controlled Salinity Waterflooding, in: *IOR 2021, European Association of*  
 20 744 *Geoscientists & Engineers, 2021: bll 1–12.* [https://doi.org/10.3997/2214-](https://doi.org/10.3997/2214-4609.202133090)  
 21 745 [4609.202133090](https://doi.org/10.3997/2214-4609.202133090).  
 22
- 23 746 [36] J. Vinogradov, M.D. Jackson, Multiphase streaming potential in sandstones saturated  
 24 747 with gas / brine and oil / brine during drainage and imbibition, *Geophys. Res. Lett.* 38  
 25 748 (2011) L01301. <https://doi.org/10.1029/2010GL045726>.  
 26
- 27 749 [37] M.-S. Kim, D.-H. Kwak, Effect of Zeta Potential on Collision-Attachment Coefficient and  
 28 750 Removal Efficiency for Dissolved Carbon Dioxide Flotation, *Environ. Eng. Sci.* 34  
 29 751 (2016) 272–280. <https://doi.org/10.1089/ees.2016.0325>.  
 30
- 31 752 [38] J.R. Moore, S.D. Glaser, H.F. Morrison, G.M. Hoversten, The streaming potential of  
 32 753 liquid carbon dioxide in Berea sandstone, *Geophys. Res. Lett.* 31 (2004) L17610.  
 33 754 <https://doi.org/10.1029/2004GL020774>.  
 34
- 35 755 [39] A. Liebscher, S. Martens, F. Moller, M. Kuhn, On-shore CO<sub>2</sub> storage at the Ketzin pilot  
 36 756 site in Germany, in: *J. Gluyas, S.B.T.-G.S. of C.D. (CO<sub>2</sub>) Mathias (Eds.), Woodhead*  
 37 757 *Publishing, 2013: bll 278–300.* <https://doi.org/10.1533/9780857097279.3.278>.  
 38
- 39 758 [40] J. Vinogradov, M.D. Jackson, M. Chamerois, Zeta potential in sandpacks: Effect of  
 40 759 temperature, electrolyte pH, ionic strength and divalent cations, *Colloids Surfaces A*  
 41 760 *Physicochem. Eng. Asp.* 553 (2018) 259–271.  
 42 761 <https://doi.org/10.1016/j.colsurfa.2018.05.048>.  
 43
- 44 762 [41] IPCC, IPCC special report on carbon dioxide capture and storage, Cambridge  
 45 763 University Press, Cambridge, 2005.  
 46
- 47 764 [42] S. Iglauer, Optimum storage depths for structural CO<sub>2</sub> trapping, *Int. J. Greenh. Gas*  
 48 765 *Control.* 77 (2018) 82–87. <https://doi.org/10.1016/j.ijggc.2018.07.009>.  
 49
- 50 766 [43] T.K. Tokunaga, DLVO-Based Estimates of Adsorbed Water Film Thicknesses in  
 51 767 Geologic CO<sub>2</sub> Reservoirs, *Langmuir.* 28 (2012) 8001–8009.  
 52 768 <https://doi.org/10.1021/la2044587>.  
 53
- 54 769 [44] T.W. Kim, T.K. Tokunaga, D.B. Shuman, S.R. Sutton, M. Newville, A. Lanzirrotti,  
 55 770 Thickness measurements of nanoscale brine films on silica surfaces under geologic  
 56 771 CO<sub>2</sub> sequestration conditions using synchrotron X-ray fluorescence, *Water Resour.*  
 57 772 *Res.* 48 (2012). <https://doi.org/10.1029/2012WR012200>.  
 58
- 59 773 [45] J. Gregory, Interaction of unequal double layers at constant charge, *J. Colloid Interface*  
 60 774 *Sci.* 51 (1975) 44–51. [https://doi.org/10.1016/0021-9797\(75\)90081-8](https://doi.org/10.1016/0021-9797(75)90081-8).

- 775 [46] K. Adamczyk, M. Prémont-Schwarz, D. Pines, E. Pines, E.T.J. Nibbering, Real-Time  
1 776 Observation of Carbonic Acid Formation in Aqueous Solution, *Science* (80-. ). 326  
2 777 (2009) 1690–1694. <https://doi.org/10.1126/science.1180060>.  
3
- 4 778 [47] C. Peng, J.P. Crawshaw, G.C. Maitland, J.P. Martin Trusler, D. Vega-Maza, The pH of  
5 779 CO<sub>2</sub>-saturated water at temperatures between 308K and 423K at pressures up to  
6 780 15MPa, *J. Supercrit. Fluids.* 82 (2013) 129–137.  
7 781 <https://doi.org/10.1016/j.supflu.2013.07.001>.  
8
- 9 782 [48] M. Kosmulski, E. Mączka, W. Janusz, J.B. Rosenholm, Multiinstrument Study of the  
10 783 Electrophoretic Mobility of Quartz, *J. Colloid Interface Sci.* 250 (2002) 99–103.  
11 784 <https://doi.org/10.1006/jcis.2002.8330>.  
12
- 13 785 [49] F. Al Saadi, K.-H. Wolf, C. Van Kruijsdijk, Characterization of Fontainebleau Sandstone:  
14 786 Quartz Overgrowth and its Impact on Pore-Throat Framework, *J. Pet. Environ.*  
15 787 *Biotechnol.* 7 (2017) 1–12. <https://doi.org/10.4172/2157-7463.1000328>.  
16
- 17 788 [50] A. Cherubini, B. Garcia, A. Cerepi, A. Revil, Influence of CO<sub>2</sub> on the Electrical  
18 789 Conductivity and Streaming Potential of Carbonate Rocks, *J. Geophys. Res. Solid*  
19 790 *Earth.* 124 (2019) 10056–10073. <https://doi.org/10.1029/2018JB017057>.  
20
- 21 791 [51] S. Li, P. Leroy, F. Heberling, N. Devau, D. Jougnot, C. Chiaberge, Influence of surface  
22 792 conductivity on the apparent zeta potential of calcite, *J. Colloid Interface Sci.* 468 (2016)  
23 793 262–275. <https://doi.org/10.1016/j.jcis.2016.01.075>.  
24
- 25 794 [52] R.M. El-Maghraby, C.H. Pentland, S. Iglauer, M.J. Blunt, A fast method to equilibrate  
26 795 carbon dioxide with brine at high pressure and elevated temperature including solubility  
27 796 measurements, *J. Supercrit. Fluids.* 62 (2012) 55–59.  
28 797 <https://doi.org/10.1016/j.supflu.2011.11.002>.  
29
- 30 798 [53] P.W.J. Glover, Geophysical Properties of the Near Surface Earth: Electrical Properties,  
31 799 *Treatise Geophys.* 11 (2015) 89–137. [https://doi.org/10.1016/B978-0-444-53802-](https://doi.org/10.1016/B978-0-444-53802-4.00189-5)  
32 800 [4.00189-5](https://doi.org/10.1016/B978-0-444-53802-4.00189-5).  
33
- 34 801 [54] L. Jouniaux, J.P. Pozzi, Streaming potential and permeability of saturated sandstones  
35 802 under triaxial stress: consequences for electrotelluric anomalies prior to earthquakes,  
36 803 *J. Geophys. Res. Solid Earth.* 100 (1995) 10197–10209.  
37 804 <https://doi.org/10.1029/95jb00069>.  
38
- 39 805 [55] J.H. Saunders, M.D. Jackson, M.Y. Gulamali, J. Vinogradov, C.C. Pain, Streaming  
40 806 potentials at hydrocarbon reservoir conditions, *Geophysics.* 77 (2012) E77–E90.  
41 807 <https://doi.org/10.1190/geo2011-0068.1>.  
42
- 43 808 [56] A.W. Islam, E.S. Carlson, Viscosity Models and Effects of Dissolved CO<sub>2</sub>, *Energy &*  
44 809 *Fuels.* 26 (2012) 5330–5336. <https://doi.org/10.1021/ef3006228>.  
45
- 46 810 [57] H. Zhao, R.M. Dillmore, S.N. Lvov, Experimental studies and modeling of CO<sub>2</sub> solubility  
47 811 in high temperature aqueous CaCl<sub>2</sub>, MgCl<sub>2</sub>, Na<sub>2</sub>SO<sub>4</sub>, and KCl solutions, *AIChE J.* 61  
48 812 (2015) 2286–2297. <https://doi.org/10.1002/aic.14825>.  
49
- 50 813 [58] H. Zhao, M. V Fedkin, R.M. Dillmore, S.N. Lvov, Carbon dioxide solubility in aqueous  
51 814 solutions of sodium chloride at geological conditions: Experimental results at 323.15,  
52 815 373.15, and 423.15K and 150bar and modeling up to 573.15K and 2000bar, *Geochim.*  
53 816 *Cosmochim. Acta.* 149 (2015) 165–189. <https://doi.org/10.1016/j.gca.2014.11.004>.  
54
- 55 817 [59] Y. Liu, M. Hou, G. Yang, B. Han, Solubility of CO<sub>2</sub> in aqueous solutions of NaCl, KCl,  
56 818 CaCl<sub>2</sub> and their mixed salts at different temperatures and pressures, *J. Supercrit. Fluids.*  
57 819 56 (2011) 125–129. <https://doi.org/10.1016/j.supflu.2010.12.003>.  
58
- 59 820 [60] D. Al Mahrouqi, J. Vinogradov, M.D. Jackson, Temperature dependence of the zeta  
60 821 potential in intact natural carbonates, *Geophys. Res. Lett.* 43 (2016) 11,578–11,587.

822 <https://doi.org/10.1002/2016GL071151>.

- 1  
2 823 [61] F.J. Millero, B. DiTrollo, A.F. Suarez, G. Lando, Spectroscopic measurements of the  
3 824 pH in NaCl brines, *Geochim. Cosmochim. Acta.* 73 (2009) 3109–3114.  
4 825 <https://doi.org/10.1016/j.gca.2009.01.037>.
- 5 826 [62] S. Datta, A.T. Conlisk, H.F. Li, M. Yoda, Effect of divalent ions on electroosmotic flow  
6 827 in microchannels, *Mech. Res. Commun.* 36 (2009) 65–74.  
7 828 <https://doi.org/10.1016/j.mechrescom.2008.07.006>.
- 9 829 [63] P.W.J. Glover, Modelling pH-dependent and microstructure-dependent streaming  
10 830 potential coefficient and zeta potential of porous sandstones, *Transp. Porous Med.*, 124  
11 831 (2018), 1573–1634. <https://doi.org/10.1007/s11242-018-1036-z>.
- 13 832 [64] L.D. Thanh, R. Sprik, Zeta potential in porous rocks in contact with monovalent and  
14 833 divalent electrolyte aqueous solutions, *Geophysics.* 81 (2016) D303–D314.  
15 834 <https://doi.org/10.1190/geo2015-0571.1>.
- 17 835 [65] X. Li, C. Peng, J.P. Crawshaw, G.C. Maitland, J.P.M. Trusler, The pH of CO<sub>2</sub>-saturated  
18 836 aqueous NaCl and NaHCO<sub>3</sub> solutions at temperatures between 308 K and 373 K at  
19 837 pressures up to 15 MPa, *Fluid Phase Equilib.* 458 (2018) 253–263.  
20 838 <https://doi.org/10.1016/j.fluid.2017.11.023>.
- 22 839 [66] B. Lorne, F. Perrier, J.-P. Avouac, Streaming potential measurements: 1. Properties of  
23 840 the electrical double layer from crushed rock samples, *J. Geophys. Res. Solid Earth.*  
24 841 104 (1999) 17857–17877. <https://doi.org/10.1029/1999JB900156>.
- 26 842 [67] M.T. Graham, D.J. MacAllister, J. Vinogradov, M.D. Jackson, A.P. Butler, Self-Potential  
27 843 as a Predictor of Seawater Intrusion in Coastal Groundwater Boreholes, *Water Resour.*  
28 844 *Res.* 54 (2018) 6055–6071. <https://doi.org/10.1029/2018WR022972>.
- 29  
30 845 [68] D. J. MacAllister, M. D. Jackson, A. P. Butler and J. Vinogradov, Tidal influence on self-  
31 846 potential measurements. *Journal of Geophysical Research - Solid Earth.*, 121 (2018),  
32 847 8432– 8452. <https://doi.org/10.1002/2016JB013376>.
- 33  
34 848 [69] M.R.S. Cabahug, E.C. Angcoy, Modeling the Reservoir Fluids of Acidic Geothermal  
35 849 Wells in Mahanagdong, Leyte, Philippines, *Procedia Earth Planet. Sci.* 7 (2013) 105–  
36 850 108. <https://doi.org/10.1016/j.proeps.2013.03.017>.
- 37  
38 851 [70] A.M. Shehata, H.A. Nasr-EI-Din, Zeta Potential Measurements: Impact of Salinity on  
39 852 Sandstone Minerals, in: *SPE Int. Symp. Oilf. Chem.*, Society of Petroleum Engineers,  
40 853 Texas, USA, 2015. <https://doi.org/10.2118/173763-MS>.
- 41  
42 854 [71] M.L. Druckenmiller, M.M. Maroto-Valer, Carbon sequestration using brine of adjusted  
43 855 pH to form mineral carbonates, *Fuel Process. Technol.* 86 (2005) 1599–1614.  
44 856 <https://doi.org/10.1016/j.fuproc.2005.01.007>.
- 45 857 [72] J.P. Kaszuba, D.R. Janecky, M.G. Snow, Carbon dioxide reaction processes in a model  
46 858 brine aquifer at 200 °C and 200 bars: implications for geologic sequestration of carbon,  
47 859 *Appl. Geochemistry.* 18 (2003) 1065–1080. [https://doi.org/10.1016/S0883-2927\(02\)00239-1](https://doi.org/10.1016/S0883-2927(02)00239-1).
- 49 860
- 50 861 [73] J.W. Morse, R.S. Arvidson, The dissolution kinetics of major sedimentary carbonate  
51 862 minerals, *Earth-Science Rev.* 58 (2002) 51–84. [https://doi.org/10.1016/S0012-8252\(01\)00083-6](https://doi.org/10.1016/S0012-8252(01)00083-6).
- 52 863
- 53  
54 864 [74] V. Bueno, A. Bosi, T. Tosco, S. Ghoshal, Mobility of solid and porous hollow SiO<sub>2</sub>  
55 865 nanoparticles in saturated porous media: Impacts of surface and particle structure, *J.*  
56 866 *Colloid Interface Sci.* 606 (2022) 480–490. <https://doi.org/10.1016/j.jcis.2021.07.142>.
- 57  
58 867 [75] R. Peng, B. Di, P.W.J. Glover, J. Wei, P. Lorinczi, P. Ding, Z. Liu, Y. Zhang, M. Wu,  
59 868 The effect of rock permeability and porosity on seismo-electric conversion: experiment



869  
1 870  
2  
3 871  
4  
5  
6  
7  
8  
9  
10  
11  
12  
13  
14  
15  
16  
17  
18  
19  
20  
21  
22  
23  
24  
25  
26  
27  
28  
29  
30  
31  
32  
33  
34  
35  
36  
37  
38  
39  
40  
41  
42  
43  
44  
45  
46  
47  
48  
49  
50  
51  
52  
53  
54  
55  
56  
57  
58  
59  
60  
61  
62  
63  
64  
65

and analytical modelling. *Geophys J. Int.* 219(1) (2019), 328–345.  
<https://doi.org/10.1093/gji/ggz249>.

### **CRedit authorship contribution statement**

**MH:** Formal analysis, Investigation, Validation, Visualization, Writing - original draft, Writing - review & editing; **MS:** Resources, Project administration, Supervision, Writing - review & editing; **JD:** Supervision, Writing - review & editing; **DVM:** Supervision; **SI:** Funding acquisition, Supervision, Writing - review & editing; **JV:** Conceptualization, Formal analysis, Resources, Funding acquisition, Methodology, Project administration, Supervision, Validation, Visualization, Writing - original draft, Writing - review & editing.

1 **Declaration of Competing Interest**

2 The authors declare no conflict of interest.